

5-2010

Commissioning an Anthropomorphic Spine and Lung Phantom for Remote Dose Verification of Institutions Participating in RTOG 0631

Douglas F. Caruthers

Follow this and additional works at: https://digitalcommons.library.tmc.edu/utgsbs_dissertations



Part of the [Other Analytical, Diagnostic and Therapeutic Techniques and Equipment Commons](#), and the [Other Physics Commons](#)

Recommended Citation

Caruthers, Douglas F., "Commissioning an Anthropomorphic Spine and Lung Phantom for Remote Dose Verification of Institutions Participating in RTOG 0631" (2010). *The University of Texas MD Anderson Cancer Center UTHealth Graduate School of Biomedical Sciences Dissertations and Theses (Open Access)*. 27.

https://digitalcommons.library.tmc.edu/utgsbs_dissertations/27

This Thesis (MS) is brought to you for free and open access by the The University of Texas MD Anderson Cancer Center UTHealth Graduate School of Biomedical Sciences at DigitalCommons@TMC. It has been accepted for inclusion in The University of Texas MD Anderson Cancer Center UTHealth Graduate School of Biomedical Sciences Dissertations and Theses (Open Access) by an authorized administrator of DigitalCommons@TMC. For more information, please contact digitalcommons@library.tmc.edu.

**Commissioning an Anthropomorphic Spine and Lung Phantom for Remote Dose
Verification of Institutions Participating in RTOG 0631**

By
Douglas Caruthers, B.S.

Approved:

Geoffrey Ibbott, Ph.D.
Supervisory Professor

Eric Chang, M.D.

David Followill, Ph.D.

Almon Shiu, Ph.D.

Allen White, Ph.D.

Approved:

Dean, University of Texas
Health Science Center at Houston
Graduate School of Biomedical Sciences

**Commissioning an Anthropomorphic Spine and Lung Phantom for Remote Dose
Verification of Institutions Participating in RTOG 0631**

A Thesis

Presented to the Faculty of
The University of Texas
Health Science Center at Houston
and
The University of Texas
M. D. Anderson Cancer Center
Graduate School of Biomedical Sciences
in Partial Fulfillment

of the Requirements

for the Degree of

MASTER OF SCIENCE

By

Douglas Caruthers, B.S.

Houston, TX
May, 2010

Acknowledgements

I would like to thank my committee, Drs. Ibbott, Followill, Chang, Shiu, and White for their guidance through the course of my research. I would like to thank the RPC physicists, Paola Alvarez and Andrea Molineu for their help with the details of my research. I would like to thank my fellow Medical Physics graduate students for all their help and support. Last, but not least, my family and Jenny for their support.

**Commissioning an Anthropomorphic Spine and Lung Phantom for Remote Dose
Verification of Institutions Participating in RTOG 0631**

Publication No.: _____

Douglas F. Caruthers
Supervisory Professor: Geoffrey Ibbott, Ph.D.

The RPC developed a new phantom to ensure comparable and consistent radiation administration in spinal radiosurgery clinical trials. This study assessed the phantom's dosimetric and anatomic utility. The 'spine phantom' is a water filled thorax with anatomy encountered in spinal radiosurgery: target volume, vertebral column, spinal canal, esophagus, heart, and lungs. The dose to the target volume was measured with axial and sagittal planes of radiochromic film and thermoluminescent dosimeters (TLD). The dose distributions were measured with the radiochromic film calibrated to the absolute dose measured by the TLD. Four irradiations were administered: a four angle box plan, a seven angle conformal plan, a seven angle IMRT plan, and a nine angle IMRT plan (denoted as IMRT plan #1 and plan #2, respectively). In each plan, at least 95% of the defined tumor volume received 8 Gy. For each irradiation the planned and administered dose distributions were registered via pinpricks, and compared using point dose measurements, dose profiles, isodose distributions, and gamma analyses. Based on previous experience at the RPC, a gamma analysis was considering passing if greater than 95% of pixels passed the criteria of 5% dose difference and 3 mm distance-to-agreement. Each irradiation showed acceptable agreement in the qualitative assessments and exceeded the 95% passing rate at the 5% / 3 mm criteria, except IMRT plan #1, which was determined to have been poorly localized during treatment administration. The measured and planned dose distributions demonstrated acceptable agreement at the 5% /

3mm criteria, and the spine phantom was determined to be a useful tool for the remote assessment of an institution's treatment planning and dose delivery regimen.

Table of Contents

Chapter 1	Introduction	1
1.1	Spinal Metastases and Radiation Therapy.....	1
1.2	The Radiological Physics Center and Remote Quality Assurance	3
1.3	Dosimeters	4
1.4	Hypothesis and Specific Aims.....	5
Chapter 2	Methods and Materials.....	6
2.1	The Spine Phantom	6
2.1.1	Schematic and Materials	6
2.1.2	Dose Measurement in the Spinal Insert.....	9
2.2	Qualitative Assessment of the Spine Phantom's Planning Utility.....	13
2.3	Phantom Simulation and Treatment Planning.....	14
2.3.1	Simulation.....	14
2.3.2	Treatment Planning System.....	14
2.3.3	Forward Treatment Planning	15
2.3.4	Inverse Treatment Planning for IMRT	16
2.4	The Treatment Plans	18
2.5	Stereotactic Positioning.....	24
2.6	Treatment Administration	26
2.7	Data Collection and Processing	27
2.7.1	TLD Dose Calculation	27
2.7.2	Film Dosimetry	30
2.7.3	Radiochromic Film Data Collection and Calibration to TLD	32

2.7.4	Exporting Dose Planes from the TPS.....	34
2.7.5	Processing and Registration of Measured Data.....	34
2.9	Data Analysis: Gamma calculations, Isodose Planes and Profiles.....	36
2.9.1	Gamma Analysis.....	37
2.9.2	Criteria Utilized	39
Chapter 3	Results and Discussion.....	41
3.1	Introduction	41
3.2	Qualitative Assessment of Anatomic Utility.....	41
3.3	TLD Measurements.....	44
3.3.1	Four-Field Box: TLD Results.....	44
3.3.2	Conformal Irradiation: TLD Results.....	46
3.3.3	IMRT #1: TLD Results	47
3.3.4	IMRT #2: TLD Results	49
3.4	Axial Profile and Isodose Distributions	51
3.4.1	Four-Field Box Plan: Isodose Distributions and Axial Dose Profile.....	52
3.4.2	Conformal Plan: Isodose Distributions and Axial Dose Profiles	55
3.4.3	IMRT #1 Plan: Isodose distributions and axial dose profile.....	56
3.4.4	IMRT #2 Plan: Isodose distributions and axial dose profile.....	59
3.5	Gamma Analysis.....	61
Chapter 4	Conclusion and Future Work.....	67
4.1	Conclusions	67
4.2	Future Work.....	70
Appendix	72

Bibliography89

List of Illustrations

Figure 2.1: An illustration of the spinal phantom with mid-axial and mid-sagittal views from CT imaging.....	7
Figure 2.2: A schematic of the axial isocenter plane of the spinal insert.....	8
Figure 2.3: A photograph of the removed spinal insert.....	9
Figure 2.4: An illustration of the sagittal and axial film slices.....	10
Figure 2.5: Schematic of the axial film slice	12
Figure 2.6: Schematic of the sagittal film slice	13
Figure 2.7: The dose distribution for the Four-Field Box plan.....	19
Figure 2.8: The dose distribution for the Conformal plan.....	20
Figure 2.9: The dose distribution for the IMRT #1 plan.....	21
Figure 2.10: The dose distribution for the IMRT #2 plan.....	22
Figure 2.11: A comparison of partial cord DVHs.....	23
Figure 2.12: Sample image of the radiochromic film used for localization of the treatment isocenter to the machine isocenter	25
Figure 2.13: The dose response curve for the batch of Gafchromic EBT film utilized.....	31
Figure 2.14: An illustration of the calibration points of the film relative to the TLDs for the axial plane.....	33
Figure 2.15: An illustration of the calibration points of the film relative to the TLDs for the sagittal plane	34
Figure 2.16: Data processing steps for film dosimetry	36
Figure 2.17: Geometric relation of points used for gamma calculation.....	38

Figure 3.1: A comparison of important anatomical distances between a male patient and the spine phantom	43
Figure 3.2: The ratio of the planned to measured dose for the Four-Field Box irradiation ...	45
Figure 3.3: The ratio of the planned to measured dose for the Conformal irradiation	47
Figure 3.4: The ratio of the planned to measured dose for the IMRT #1 irradiation.....	48
Figure 3.5: The ratio of the planned to measured dose for the IMRT #2 irradiation.....	50
Figure 3.6: Illustration of the axial dose profile location	52
Figure 3.7: Isodose distributions for the axial and sagittal planes of the Four-Field Box irradiation.....	53
Figure 3.8: Axial dose profile: Four-Field Box irradiation	54
Figure 3.9: Isodose distributions for the axial and sagittal planes of the Conformal irradiation	55
Figure 3.10: Axial dose profile: Conformal irradiation	56
Figure 3.11: Isodose distributions for the axial and sagittal planes of the IMRT #1 irradiation	57
Figure 3.12: Axial dose profile: IMRT #1 irradiation.....	58
Figure 3.13: Isodose distributions for the axial and sagittal planes of the IMRT #2 irradiation	59
Figure 3.14: Axial dose profile: IMRT #2 irradiation.....	60
Figure 3.15: Gamma analysis maps of the axial and sagittal planes for the first trial of the Four-Field Box irradiation.....	62
Figure 3.16: Gamma analysis map of the axial and sagittal planes for the first trial of the Conformal irradiation.....	63

Figure 3.17: Gamma analysis maps of the axial and sagittal planes for the second trial of the IMRT #1 irradiation	64
Figure 3.18: Gamma analysis maps of the axial and sagittal planes for the first trial of the IMRT #2 irradiation	65
Figure 4.1: The mean percentage of pixels passing the gamma criteria for each anatomic plane for each irradiation type.	69
Figure 5.1: Isodose distributions for the axial and sagittal planes of the Four Field Box irradiation, Trial 2	73
Figure 5.2: Gamma analysis maps of the axial and sagittal planes for the Four-Field Box irradiation, Trial 2	74
Figure 5.3: Isodose distributions for the axial and sagittal planes of the Four Field Box irradiation, Trial 3	75
Figure 5.4: Gamma analysis maps of the axial and sagittal planes for the Four-Field Box irradiation, Trial 3	76
Figure 5.5: Isodose distributions for the axial and sagittal planes of the Conformal irradiation, Trial 2	77
Figure 5.6: Gamma analysis maps of the axial and sagittal planes for the Conformal irradiation, Trial 2	78
Figure 5.7: Isodose distributions for the axial and sagittal planes of the Conformal irradiation, Trial 3	79
Figure 5.8: Gamma analysis maps of the axial and sagittal planes for the Conformal irradiation, Trial 3	80
Figure 5.9: Isodose distribution of the sagittal plane of the IMRT #1 irradiation, Trial 1.....	81

Figure 5.7: Isodose distributions for the axial and sagittal planes of the Conformal irradiation, Trial 3	81
Figure 5.10: Gamma analysis map of the sagittal plane of the IMRT #1 irradiation, Trial 1	82
Figure 5.11: Isodose distributions for the axial and sagittal planes of the IMRT #1 irradiation, Trial 3	83
Figure 5.12: Gamma analysis maps of the axial and sagittal planes for the IMRT #1 irradiation, Trial 3	84
Figure 5.13: Isodose distributions for the axial and sagittal planes of the IMRT #2 irradiation, Trial 2	85
Figure 5.14: Gamma analysis maps of the axial and sagittal planes for the IMRT #2 irradiation, Trial 2	86
Figure 5.15: Isodose distributions for the axial and sagittal planes of the IMRT #2 irradiation, Trial 3	87
Figure 5.16: Gamma analysis maps of the axial and sagittal planes for the IMRT #2 irradiation, Trial 3	88

List of Tables

Table 3.1: The absorbed dose to TLD at each position for the Four- Field Box irradiation..	45
Table 3.2: The absorbed dose to TLD at each position for the Conformal irradiation.....	46
Table 3.3: The absorbed dose to TLD at each position for each trial for the IMRT #1 irradiation.....	48
Table 3.4: The absorbed dose to TLD at each position for each trial for the IMRT #2 irradiation.....	49
Table 3.5: The mean percentage of pixels passing the gamma criteria for each dose plane in each irradiation.....	66

Chapter 1 Introduction

1.1 Spinal Metastases and Radiation Therapy

The spine is the most common site for bony metastases. An estimated 40% of cancer patients develop spinal metastases, and approximately 10-20% of these patients suffer symptomatic spinal cord compression from these lesions. This amounts to more than 25,000 cases per year. Approximately 70% of spinal tumors originate from a primary tumor elsewhere in the body, the majority from primary cancers of the lung, breast, and prostate. Lesions can also originate in the spine; these include meningiomas, schwannomas, osseous tumors, and gliomas. Spinal cord compression often presents with back pain, instability, and neurologic deficit (Klimo 2004).

Management of spinal tumors includes radiation, surgery, and chemotherapy. The role of radiation has evolved with developments in diagnostic imaging, inverse treatment planning, image-guided therapy, and intensity modulated radiation therapy (IMRT). As more institutions across the country are able to deliver highly conformal doses with smaller margins of error, hypo-fractionated and single-fraction treatments for spinal tumors show increasing promise as a new standard of care. This type of approach, when applied to the head and spine, falls under the banner of ‘stereotactic radiosurgery’ (SRS). This term, coined by Lars Leksell in the 1950’s, was based on combining an intracranial guidance device and an orthovoltage X-ray unit. Since then, the term has come to encompass techniques for delivering a high dose of radiation in a small number of fractions (< 5) with a high degree of spatial accuracy using image guidance and immobilization (Dodd 2008). In the literature, spinal radiosurgery is often categorized under SRS or under stereotactic body radiotherapy

(SBRT). In this paper, radiation delivered to spinal tumors in a single fraction with image guidance and immobilization will be referred to as spinal radiosurgery.

A previous Radiation Therapy Oncology Group (RTOG) trial established that a single dose of 8 Gy accomplished the same degree of pain relief as 10 fractions of 3 Gy (a total dose of 30 Gy) (RTOG 2009). However, these results were based on conventional administration of radiation (non-IMRT). The optimum dose level using ‘dose-painting’ techniques for spinal metastases is actively under investigation (RTOG 2009). Ryu et al. treated patients with image-guided radiosurgery on a BrainLAB (Westchester, IL) Novalis® system (treatments were intensity modulated with a micro MLC); these patients received single fraction doses of 10 to 16 Gy, and achieved an overall pain control rate for one year of 84% (Ryu 2008). Gerszten et al. described the success they had with single fraction dose, delivered on an Accuray (Sunnyvale, CA) Cyberknife® system (a cylindrically collimated linac on an articulating robotic arm), from 12.5 to 25 Gy; 290 of their 336 cases achieved long term pain improvement (Gerszten 2007). Chang et al. treated 74 patients with metastatic spinal lesions with IMRT and near simultaneous CT guidance; these patients received 6 Gy in 5 fractions, later amended to 9 Gy in 3 fractions. Chang et al. reported 84% progression free incidence after 1 year (Chang 2007). These studies described the benefit achieved at escalated dose levels; however, there has been a dearth of prospective studies on the benefit of an escalated prescription level. This dearth is being addressed by the Radiation Therapy Oncology Group (RTOG). The RTOG is currently enrolling patients into protocol 0631, a phase II/III study of image-guided radiosurgery/stereotactic body radiotherapy for localized spine metastases. This protocol randomizes patients into two arms. The first arm treats patients with an escalated dose level in a single fraction (16 Gy) delivered via ‘dose-

painting' techniques (such as IMRT); the second arm uses a single fraction at a lower dose level (8 Gy) delivered conventionally (non-IMRT). Both arms of the protocol require image guidance and immobilization in order to ensure treatment accuracy (RTOG 2009).

1.2 The Radiological Physics Center and Remote Quality Assurance

The Radiological Physics Center's (RPC) mission is "to assure NCI and the Cooperative Groups that institutions participating in clinical trials deliver prescribed radiation doses that are clinically comparable and consistent."

The RPC accomplishes this mission in several ways: machine output checks with mailed TLD, dose algorithm checks on reference patients, quality assurance procedure reviews, on-site dosimetry review visits, credentialing for participation in clinical trials, and retrospective reviews of an institution's treatment records. The RPC also utilizes anthropomorphic phantoms for remote quality assurance. The RPC employs head and neck, thorax, and pelvic phantoms, among others. Typically, the phantoms are water-filled and contain materials of different densities in simple geometries to model the anatomy of interest. Dosimetry is accomplished using film and thermoluminescent dosimeters (TLD) loaded into the organs-at-risk and the treatment volumes. The phantoms are mailed to institutions participating in clinical protocols. The institution irradiates the phantom according to their treatment plan and procedures, and sends the phantom back to the RPC. The RPC then assesses the delivered dose (measured via the radiochromic film and TLD) to ensure it conforms both to the prescribed treatment plan and to standards set forth by a given protocol. This process enables the RPC to verify an institution's entire treatment process: imaging,

planning, dose calculation, positioning, and dose delivery, before treatments are administered to patients.

The RTOG Protocol 0631 falls under the RPC's purview. The RPC designed a new phantom to address this new clinical protocol. The materials, anatomical layout and dose measurement geometry of this new phantom are described more fully in the Methods and Materials section. Essentially, the new phantom, denoted herein as the 'spine phantom', is a water-filled anthropomorphic chest with low-density lungs and a spine insert that simulates the spinal cord, vertebral column, esophagus, and target volume.

However, the utility of this newly designed and manufactured spine phantom has to be verified before it can be used as a dosimetry tool by the RPC. This work tested the utility of the spine phantom. Both the anatomic utility and dosimetric utility were assessed. The planning utility concerned how well the spine phantom represented the challenges of planning spinal irradiations in the layout and proportion of the organs-at-risk and target volumes. The dosimetric utility concerned whether TLD and radiochromic film recovered from the phantom consistently measured the administered dose. Establishing the dosimetric utility was accomplished through the administration of radiation treatment plans of varying complexity, and assessing how well the results, measured via radiochromic film and TLD, agreed with the planned dose distribution.

1.3 Dosimeters

The remote dosimetry system utilized by the RPC is a combination of radiochromic film and thermoluminescent dosimeter (TLD). The radiochromic film used in this project was Gafchromic EBT film, manufactured by International Specialty Products (Columbia,

MD). The optical density (OD) of the radiochromic film increases as a function of dose, and does not require development. The film was used to measure relative dose distributions. The TLD measured an absolute dose to a small volume, to which the relative dose distribution was calibrated. The system is discussed in more detail in Methods and Materials section.

1.4 Hypothesis and Specific Aims

Hypothesis:

The newly constructed spine phantom provides a useful model for planning intensity modulated radiosurgery for spinal tumors, and the collapsed-cone convolution dose algorithm accurately models the dose distributions measured via radiochromic film and TLD.

This hypothesis was tested by the following specific aims:

Specific Aims:

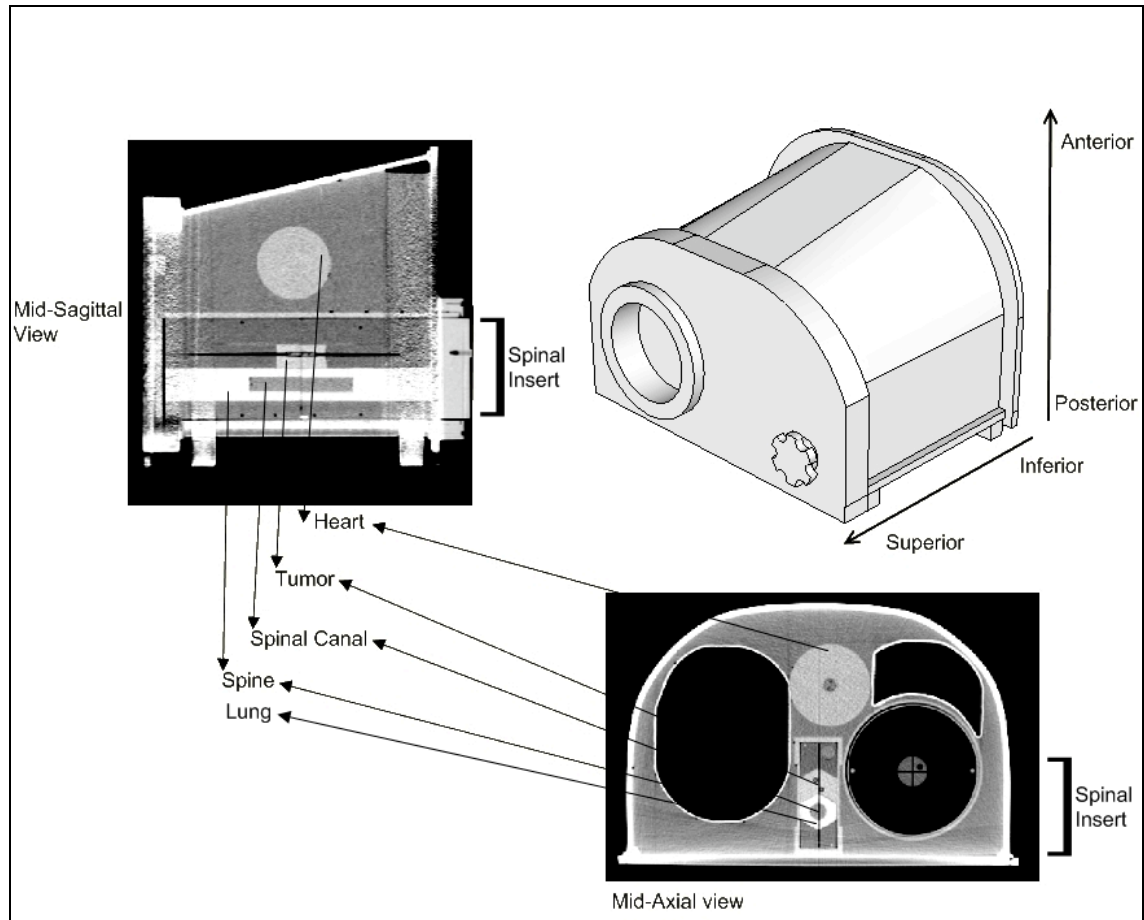
1. Qualitatively assess the anatomic layout of the spine phantom and how well it models anatomical features of a patient of similar chest breadth.
2. Develop treatment plans that do not use intensity modulation to irradiate the treatment volume to the relevant prescription dose.
3. Develop intensity-modulated treatment plans with clinically relevant prescription dose to the planned tumor volume and clinically relevant dose constraints on the organs at risk.
4. Compare the planned and measured dose distributions with quantitative and qualitative assessments: point dose, dose profiles, and isodose distributions.
5. Compare the planned and measured dose distributions using a gamma analysis

Chapter 2 Methods and Materials

2.1 The Spine Phantom

2.1.1 Schematic and Materials

The spine phantom has overall dimensions of 40 cm width by 30 cm height by 30 cm length. The outer shell is a 6 mm thick shell of polyvinyl chloride. Inside the shell, a nylon sphere serves as the heart. The left lung is a removable cylindrical compressed cork insert with a tumor feature; this phantom also serves as a remote quality assurance tool for lung protocols. The right lung is permanent, and is also made of compressed cork. A large hole with a sealing screw cap is located on the superior end of the phantom for water filling. Any portion of the inner cavity of the shell not occupied by anatomy fills with water; this serves the dual purpose of near tissue equivalence and provides ease of handling the unfilled phantom. These features are illustrated in Figure 2.1.



Anatomy:	Material	Density (g/cm ³)
Heart	Nylon	1.06
Tumor	Acrylic	1.07
Spine	Polystyrene	1.2
Spinal Canal	Solid Water	1.03
Lung	Cork	0.3

Figure 2.1: An illustration of the spinal phantom with mid-axial and mid-sagittal views from CT imaging. The anatomical features are labeled and the materials and densities listed in the table above.

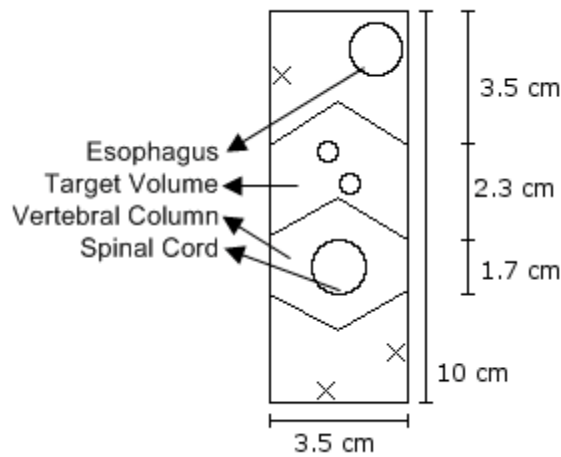


Figure 2.2: A schematic of the axial isocenter plane of the spinal insert. The crosses denote the pin-prick locations used for localization.

The spine insert was designed and built at the RPC based on the anatomy of sample patients selected as representative cases for spinal radiosurgery. The spinal insert, highlighted in Figure 2.1, is loaded inferiorly into the spine phantom, and has dimensions of 30 cm by 10 cm by 4 cm. The insert runs the length of the phantom, between the posterior portions of the lungs. When inserted, the insert locks into place with screws for reproducible placement. The insert contains pertinent anatomy for spinal irradiations: spinal cord, esophagus, vertebral column, and a target volume, the anatomical features are shown in Figure 2.2. The materials chosen for these anatomical features roughly correspond to anatomical densities, and are detailed in section 3.2. The different materials provide CT contrast for ease of anatomical contouring.

2.1.2 Dose Measurement in the Spinal Insert

The spinal insert, when removed, disassembles into a superior and inferior portion, depicted in the Figure 2.3. The disassembled portions of the spinal insert bisect the acrylic tumor volume.

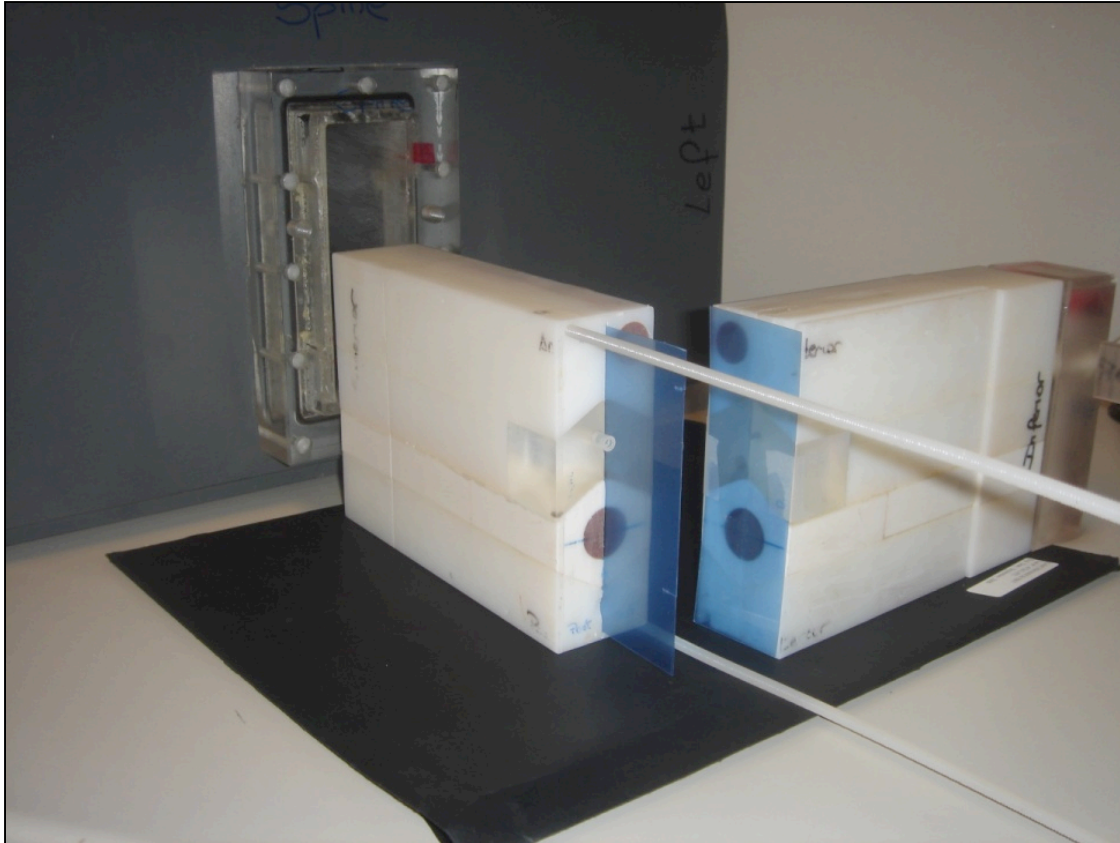


Figure 2.3: A photograph of the removed spinal insert. To illustrate the relative location of the film planes, radiochromic film was placed on the sagittal and axial planes of the disassembled insert. Also, the different materials used in the construction of the anatomy of interest are visible.

The radiochromic film was cut exactly to the axial dimensions of the spinal insert. Three pins are embedded in the axial face of the dissembled spinal insert. When placed onto the axial plane of the spinal insert, the radiochromic film is pierced by the pins, registering

the axial film slice to the fixed geometry of the pins. For the sagittal dose plane, slices were machined into the spine insert, creating a thin sagittal plane bisecting the tumor volume. Radiochromic film was inserted into these cuts for sagittal dose distribution measurement. Once inserted, the sagittal film slices can be registered with pinpricks through holes that traverse the spine insert, perpendicular to the sagittal film plane. The pin-pricks on the film correspond to the known geometry of the holes for registration.

Figure 2.4 shows the relation of the axial and sagittal film planes in the spine insert and the relative location of the TLD capsules. The varied spatial position of the TLD capsules within the target volume provided measurements of absolute dose at various depths.

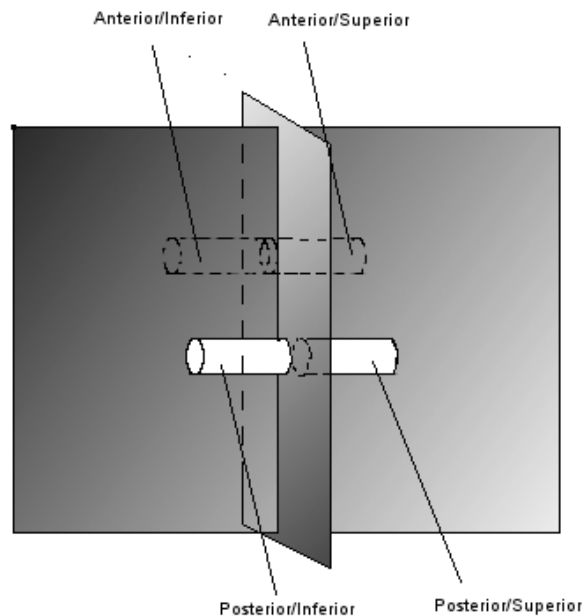


Figure 2.4: An illustration of the sagittal and axial film slices (the axes of the TLD capsules run parallel to the sagittal film); each TLD capsule is located within the PTV, and their locations relative to the target volume center are labeled.

The radiochromic film utilized in this project, Gafchromic EBT, has properties that make it ideal for use in remote quality assurance applications. The film requires no

development, and can be cut to any shape required by the dimensions of the film plane. The film is insensitive to visible light, allowing for ease of use and portability. The radiochromic film has a high spatial resolution allowing for the measurement of the steep dose gradients used in spinal radiosurgery. The film can also be calibrated over a clinically useful range of doses (up to 10 Gy), is water equivalent, and the response is independent of energy and dose rate. Fuss et al. also found the film response independent of beam quality by irradiating the film at different depths. This characteristic is particularly useful, as calibration of the film need not be conducted at the depth at which it is placed in the phantom. The main caveat for use of Gafchromic EBT film is that it continually develops; thus, it is not well suited to permanent storage of dose data (Fuss 2007).

The film was cut to the required size and shape for the spine phantom. The following schematics in Figures 2.5 and 2.6 show the size of the films utilized and the locations of registration markings:

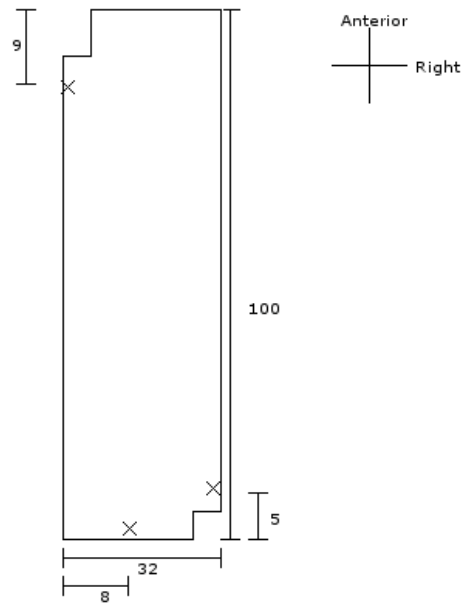


Figure 2.5: Schematic of the axial film slice. All measurements are in millimeters. The crosses denote the position of the registration pin locations.

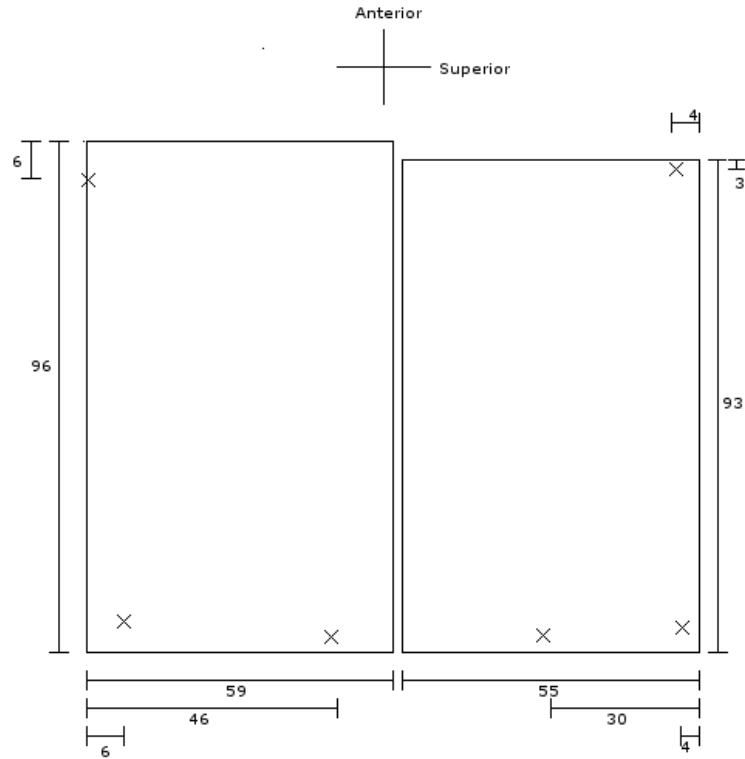


Figure 2.6: Schematic of the sagittal film slice. All measurements are in millimeters. The crosses denote the position of the registration pin locations.

2.2 Qualitative Assessment of the Planning Utility of the Spine Phantom

The spine phantom will serve the purpose of assessing an institution's ability to image, develop a treatment plan, and deliver the stereotactic plan. An important component of the utility of the phantom in this assessment is that it presents a reasonable simulation of spinal anatomy. Granted, there is no one 'correct' anatomy for a spine and spine tumor; spinal tumors vary greatly in size and presentation. Tumors may involve multiple levels, range greatly in mass, and proximity to the spine. However, it is still critical that the design of the spine phantom be representative in a few categories: depth, size, and proximity to the spinal cord.

To assess how well the spine phantom conforms to these criteria, CT scans for a patient with comparable chest breadth to the spine phantom were acquired, and measurements were taken of pertinent critical anatomy. This process allowed for a reasonable qualitative assessment of the anatomic utility of the spine phantom.

2.3 Phantom Simulation and Treatment Planning

2.3.1 Simulation

The phantom was simulated on a Philips AcQsim CT scanner. Prior to scanning, film and TLD were loaded into the phantom. The phantom was filled with water, with care taken to avoid air bubbles (the design of the phantom, with a sloping chest, prevented air bubbles from being near the treatment fields). The following parameters were used in the acquisition: 120 kVp, dynamic mAs, and 1.5 mm slice thickness. The simulation system allowed for landmarking of the target isocenter during the simulation. Once landmarked, the CT couch then shifted the room lasers for external marking of the simulation isocenter. Three plastic fiducials were used to mark the laser positioning for an approximate treatment setup.

2.3.2 Treatment Planning System

The Philips “Pinnacle” treatment planning system (TPS), version 7.6, was utilized for the design of each treatment plan administered to the spine phantom. This TPS utilized a set of M.D. Anderson’s standard institutional beam data for the Varian 2100 linear accelerators. These beam data are the clinical standard at M.D. Anderson. For IMRT planning, the TPS employed an inverse planning algorithm; for a given beam arrangement and set of dose parameters, the TPS calculated the optimal step-and-shoot MLC fields and the monitor units

for each field. The planning process involved the incremental optimization of a plan until it is clinically acceptable.

Pinnacle 7.6 was also utilized for the forward-planning process of a set of simple-beam arrangements plans. In this planning process, the field shapes, beam arrangements, and beam weighting were set by the user; the TPS then calculated the necessary monitor units to irradiate the target volume to the prescription dose.

The planned dose was calculated with the collapsed-cone convolution algorithm implemented in Pinnacle. This dose algorithm is the clinical standard at M.D. Anderson. The algorithm addressed the heterogeneity in the phantom (it does not assume a uniform density of water, but calculated dose based on the CT number of the scanned phantom). Addressing heterogeneity is important in the spine phantom because, depending on the beam arrangement, a significant portion of the beam passes through high density simulated bone material and low density simulated lung material.

2.3.3 Forward Treatment Planning

Four different treatment plans were developed for the spine phantom. In each plan, a prescription dose level of 8 Gy was utilized. This dose level is not at the prescription level delineated in the RTOG 0631 protocol (which escalates the dose to 16 Gy). This lower dose level was chosen to keep the prescription within the dosimetric range of the radiochromic film.

First, a four beam plan was created; beams were placed anteriorly, posteriorly, left, and right (IEC convention: 0°, 180°, 270°, and 90°). The planning target volume (PTV) was the acrylic tumor contour expanded by 1 mm. A dose of 8 Gy was prescribed to 95% of the

PTV with equal beam weighting. This plan will be referred to herein as the four-field box plan.

Next, a conformal plan was developed. Seven beams were arranged posteriorly (90° , 120° , 150° , 180° , 210° , 240° , and 270°). The acrylic tumor contour was expanded 1 mm. The plan was conformal; each beam was collimated with the multi-leaf collimator to the planning target volume. 8 Gy was prescribed to 95% of the PTV. This plan will be referred to herein as the conformal plan.

The four-field box and conformal plans had no intensity modulation. These plans were developed to help establish the baseline agreement between planned and measured dose. Venselaar et al. demonstrated that, for simple beam geometries with larger field sizes, the accuracy of the treatment planning calculation was greater (Venselaar 2001). These plans had less clinical significance because they ignored spinal cord dose constraints in favor of simplicity in design, ease of administration, and measurement accuracy.

2.3.4 Inverse Treatment Planning for IMRT

Next, two intensity modulated plans were developed. Two different beam arrangements were utilized; one borrowed from the treatment plan for a patient at M.D. Anderson, the other with a beam arrangement optimized for the irradiation of spinal metastases (Pugachev 2001). The dose constraints for the anatomy of interest were taken from the RTOG protocol 0631 (RTOG 2009). The pertinent constraints from the protocol are listed in Table 2.1.

Critical Structures and Dose Constraints	<i>Critical Volume</i>	<i>Max. Dose to Critical Volume</i>	<i>Max. Point Dose To Critical Volume</i>
<i>Spinal Cord</i>	10% / 3%	3.5 Gy / 5 Gy	7 Gy
<i>Esophagus</i>	15%	6 Gy	8 Gy
<i>Lungs</i>	20%	3.7 Gy	

Table 2.1: *The critical structures and the dose/volume constraints for each delineated by the RTOG protocol 0631.*

In Philips' Pinnacle treatment planning software, the dose constraints for the critical structures were entered into the inverse treatment planning software. Each dose constraint was assigned a weighting factor. In spinal radiosurgery, the spinal cord is the limiting factor for higher levels of dose to the target volume, due to its proximity (in the spine phantom, the spinal cord is 7 mm posterior to the target volume) and the devastating nature of radiation induced myelopathy (Dodd 2008).

With the beams arranged and the dose constraints assigned, the TPS optimized the modulated, step-and-shoot MLC fields for achieving the specified dose distribution. Once the software created the plan, the dose distribution and dose-volume histograms were assessed. Then, the weightings were adjusted, and the plan re-optimized. This iteration continued until the resultant plan satisfied the user's criteria (Holder 2004).

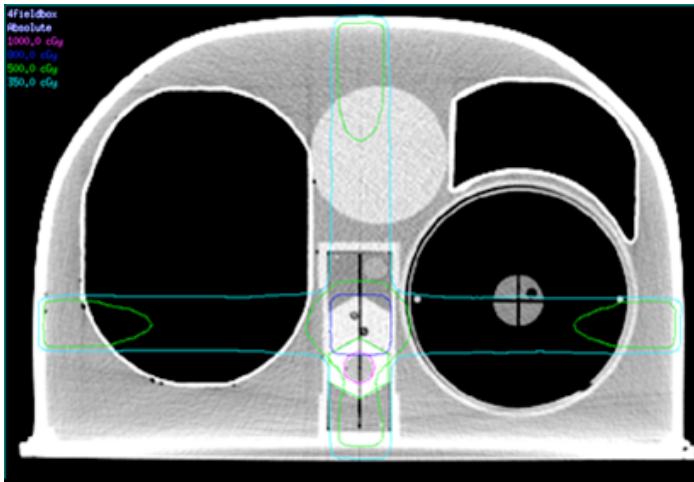
Two IMRT plans were developed, the dose distributions are shown in Figure 2.9 and 2.10. The first plan did not satisfy the clinical constraints; however, this plan still yielded insight into how well the internal dose-measurement system agreed with the calculated dose distribution. The second plan satisfied the clinical constraints set forth by the protocol. This plan was the type of plan that may be administered by institutions participating in the protocol.

The first IMRT plan utilized 6 MV photons and seven fields; the beam angles were 100°, 120°, 150°, 180°, 200°, 230°, and 260°. This plan will be referred to herein as IMRT plan #1.

The second IMRT plan also utilized 6 MV photons, but used nine fields; the beam angles 60°, 105°, 130°, 150°, 165°, 180°, 210°, 230°, and 280°. This plan will be referred to herein as IMRT plan #2.

2.4 The Treatment Plans

The following images in Figures 2.7-2.10 show the dose distributions on the axial CT slices of the spine phantom at isocenter. The beam arrangement and number of monitor units per field are listed below the dose distribution image. The prescription dose for each plan was 8 Gy to at least 95% of the volume of the PTV.



Four-Field Box:				
Beam #	1	2	3	4
Gantry Angle:	0	270	180	90
MU's:	343	343	343	343

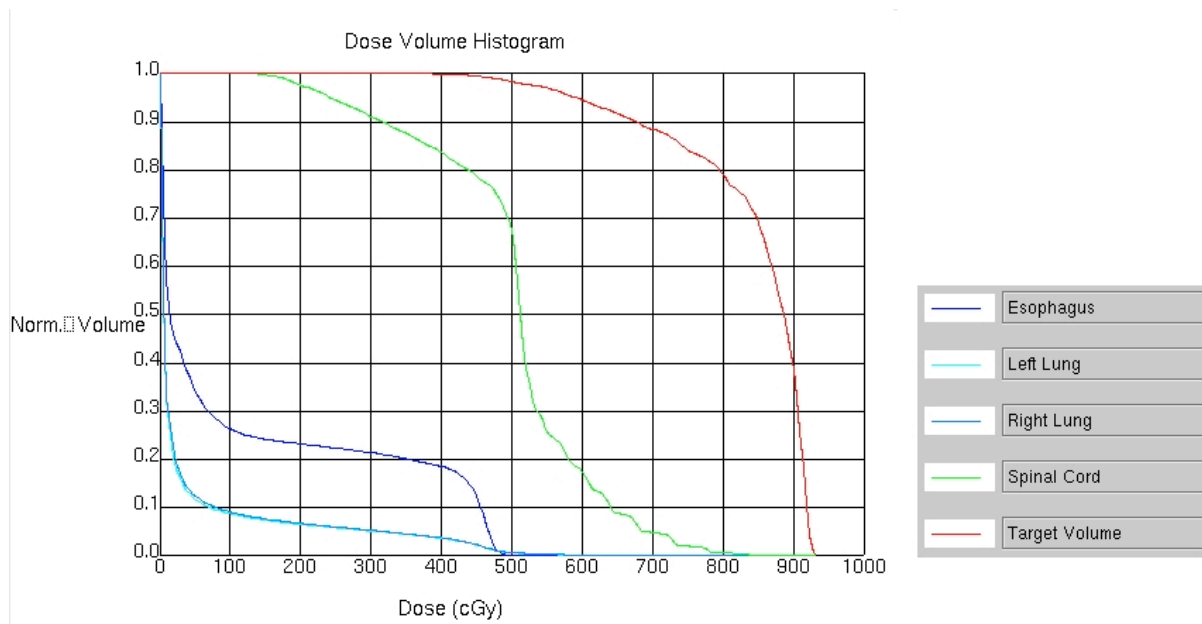
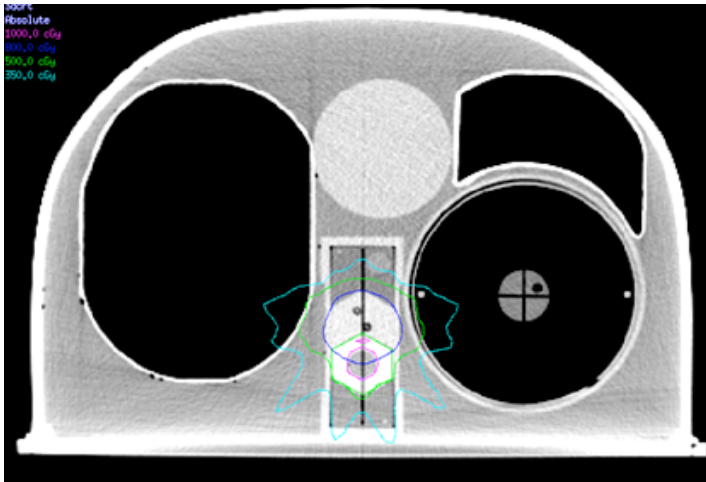


Figure 2.7: The dose distribution for the four-field box plan; the gantry angles and numbers of monitor units per field are shown. Below the table are the dose volume histograms for the critical structures.



Conformal:							
Beam #	1	2	3	4	5	6	7
Gantry Angle:	270	240	210	180	150	120	90
MU's:	197	197	197	197	197	197	197

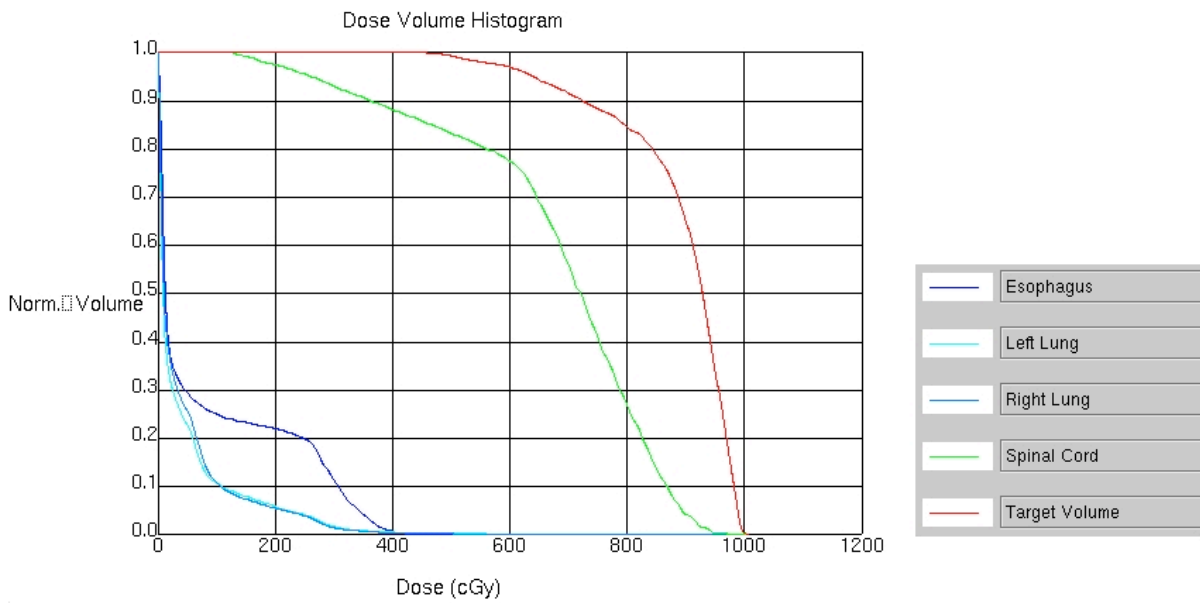
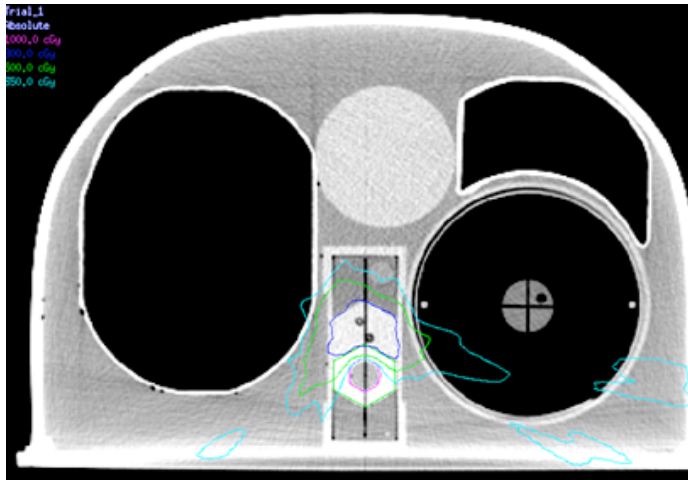


Figure 2.8: The dose distribution for the conformal plan; the gantry angles and number of monitor units per field are shown. Below the table are the dose volume histograms for the critical structures.



IMRT #1:							
Beam #:	1	2	3	4	5	6	7
Gantry Angle:	260	230	200	180	150	120	100
MU's:	302	429	340	376	187	461	551

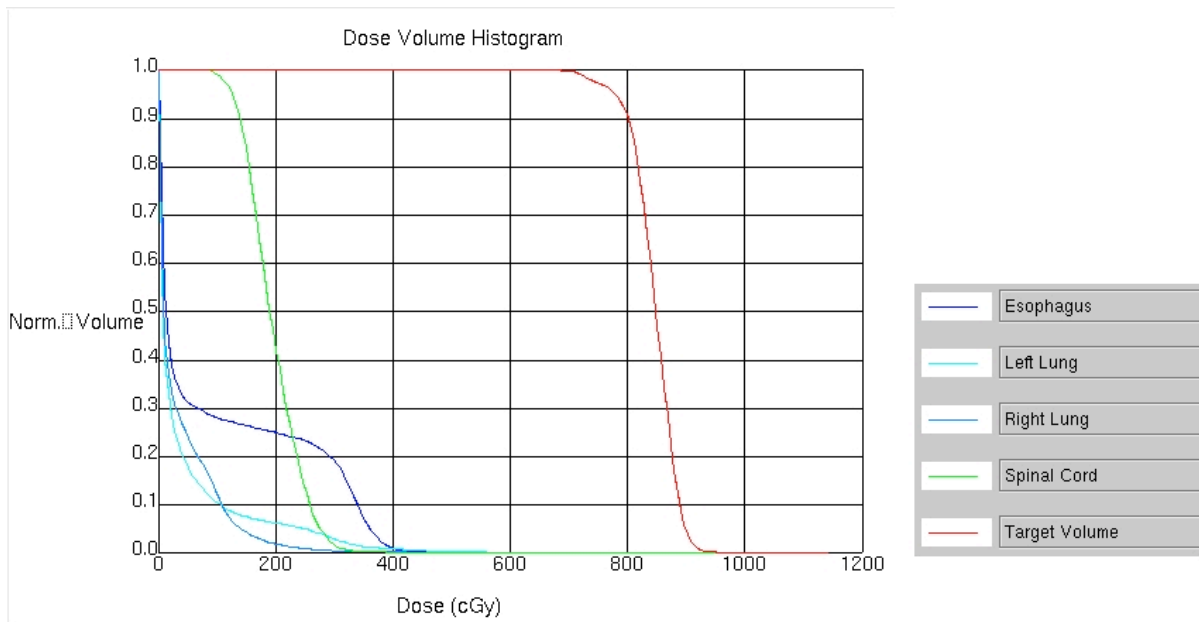
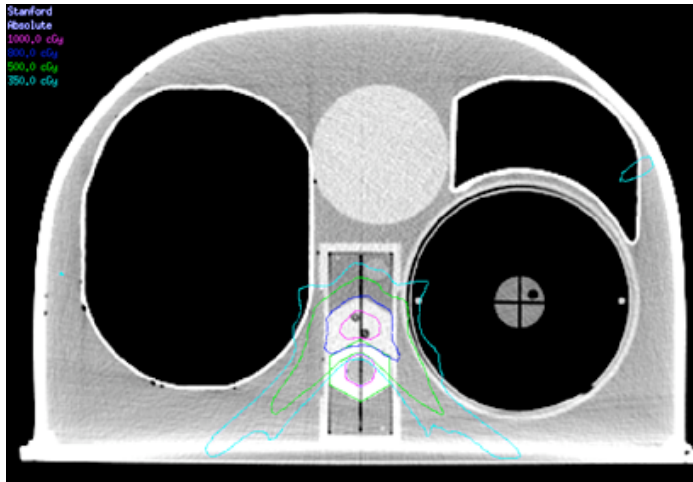


Figure 2.9: The dose distribution for the IMRT plan #1; the gantry angles and numbers of monitor units per field are shown. Below the table are the dose volume histograms for the critical structures.



IMRT #2:									
Beam #:	1	2	3	4	5	6	7	8	9
Gantry Angle:	280	230	210	180	165	150	130	105	60
MU's	310	366	314	322	485	321	414	266	365

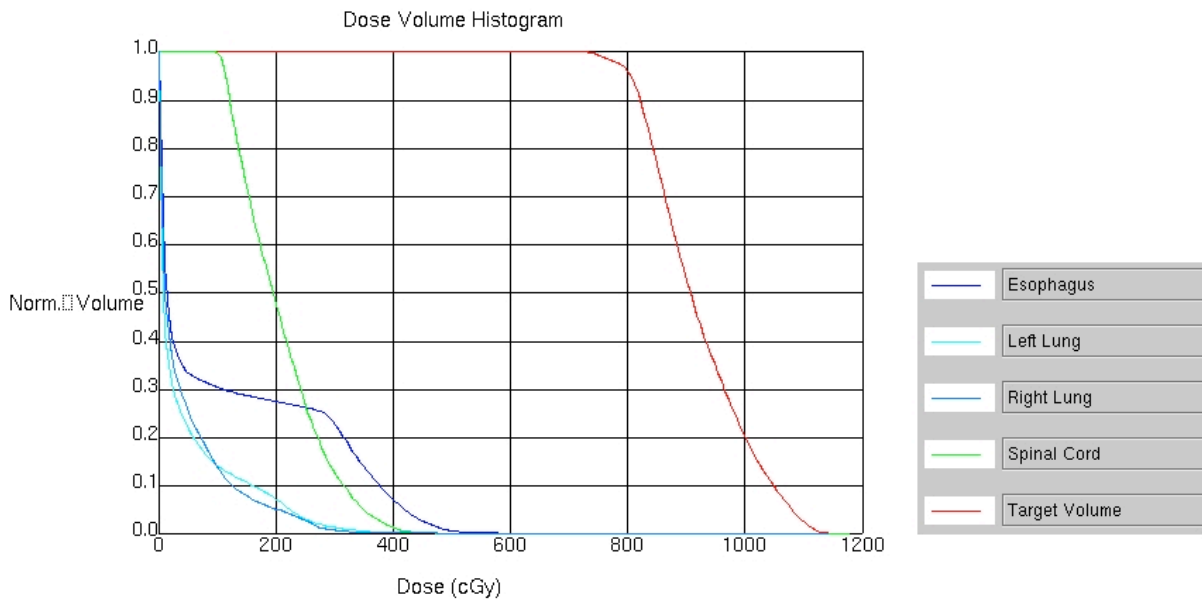


Figure 2.10: The dose distribution for the IMRT plan #2; the gantry angles and numbers of monitor units per field are shown. Below the table are the dose volume histograms for the critical structures.

IMRT plan #2 met the constraints set forth by the RTOG 0631 protocol. The cumulative dose-volume histogram of the spinal cord was compared to the average DVH from a study conducted by Ryu et al. Figure 2.11 plots the DVH of IMRT plan #2 along with the average spinal cord DVH for 50 patients from Ryu's study. The comparison is appropriate, as the partial cord volume was defined the same for Ryu's patients and for the IMRT plan #2 treatment.

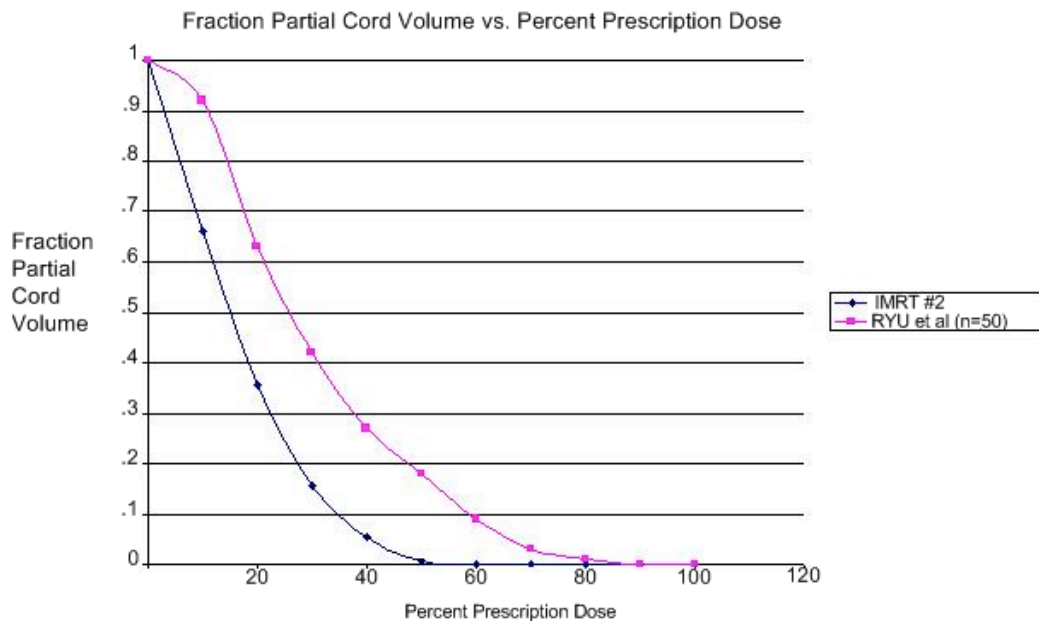


Figure 2.11: A comparison of the partial cord DVH from the treatment plan utilized in this study and the average DVH across 50 patients measured by Ryu et al.

The graph demonstrates that IMRT plan #2 achieved a dose-volume histogram for the spinal cord that satisfies the requirements of the protocol, and has a lower cord dose at all fractions of the partial cord volume when compared to clinical findings (Slotman 2006). The DVH for the spinal cord may be significantly lower than that of the Ryu et al. study because of the 7 mm gap between the spinal cord and the target volume (it is more than

twice the minimal proximity in RTOG 0631, 3 mm, under which patients are excluded); the spine phantom may represent a relatively easy planning challenge to institutions participating in RTOG 0631.

2.5 Stereotactic Positioning

In radiosurgery, positioning must be accurate with a high level of confidence. The RTOG protocol 0631 calls for 0-3 mm margins around the PTV. For these plans, the margin used was 1 mm. Image guidance is a prerequisite for entry into RTOG Protocol 0631. Participating institutions approach radiosurgery with a variety of positioning solutions. Typically, these involve the use of orthogonal kV imaging, followed by table shifts and position checks. Other approaches include cone-beam CT or CT on rails. The common theme is the utilization of imaging of anatomical structures at the time of treatment (Chen 2009).

The rigidity of the phantom negated part of the positioning problem, as positioning is not compromised once the phantom is in place. This rigidity obviates the use of stabilization devices used in radiosurgery, such as the Elekta (Stockholm, Sweden) BodyFIX® system.

For the irradiations conducted in this study, an alternate approach to image guided positioning was devised to ensure accuracy. First, the location of the treatment isocenter, noted from the TPS, was marked on a set of sagittal and axial radiochromic films. These films were then loaded into the spinal insert, and the spinal insert was loaded into the phantom. The phantom was set to an initial position according to external fiducials placed during simulation on the patient support table. Then, a series of irradiations were

administered with the collimator jaws set to a 1 mm gap. The gantry and collimator angles were varied at 90° increments, creating a cross pattern on the radiochromic film. The spinal insert was removed, and a shift was calculated between the machine isocenter (the center of the cross pattern) and the treatment isocenter (marked on the film), and this shift was applied to the patient support table. This process was iterated until there was exact coincidence between the machine and treatment isocenters. An image of an iteration of this process is shown in Figure 2.12.

This procedure is analogous to a hidden target test, described in AAPM TG-42. In these types of tests, a lead or steel bearing is located at the treatment isocenter, and deviations from the machine isocenter are measured (Schell 1995). In the localization technique for the spine phantom described above, these deviations were measured, and then corrected for with a patient support table shift.

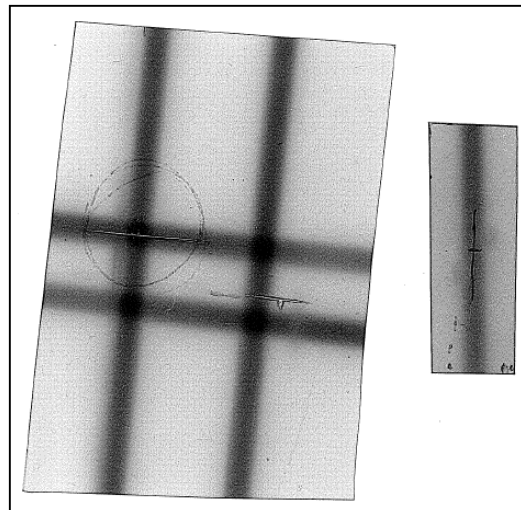


Figure 2.12: Sample image of the radiochromic film used for localization of the treatment isocenter to the machine isocenter. For the 1 mm wide fields, a 1.5 mm wide region developed on the film. After each irradiation, the shift was calculated and applied;

this process was iterated until the treatment isocenter coincided with the machine isocenter.

This approach provided accurate positioning of the treatment isocenter to the machine isocenter. Although institutions being credentialed cannot use this process for positioning, the goal of this project was to assess the agreement of the planned dose distribution to the measured dose distribution; error introduced by positioning uncertainty from image guidance may have confounded the results. This localization procedure bypassed the positioning uncertainty introduced by image guided positioning.

2.6 Treatment Administration

Once in position, the phantom was ready for treatment. The spinal insert was loaded with film and TLD, and the MLC fields were loaded into the controller. After checking the clearance of the linear accelerator around the spine phantom, the treatment started. In order to bypass the record and verify system, the plans were delivered manually. Since the treatment administration was manual, the gantry angle, collimator angle, number of monitor units, and dynamic MLC file had to be loaded for each beam. No safety interlocks prevented administration of the wrong field at the wrong angle, so a double-tiered checklist was utilized to prevent error.

Each treatment plan was administered three times. Between each trial, the spine insert was removed, and new TLD and film were placed in the insert. A long pin was used to pierce the film for registration in the sagittal aspect. The phantom was not re-positioned between trials.

2.7 Data Collection and Processing

The RPC has a long history using TLD for dosimetry; it has been an essential component of the remote quality assurance regimen for 30 years. Since 1996, TLDs have been implemented in anthropomorphic phantoms. Kirby et al. described the uncertainties in a powder TLD system, and ascribed a +/-5% action criterion for TLD checks, corresponding to a 93% confidence interval (Kirby 1992).

TLD-100, manufactured by the Radiation Detection Company in Gilroy, CA, was utilized in these experiments. The TLD powder is placed in custom made cylindrical capsule measuring 15 mm in length and 4 mm in diameter. The wall thickness of the capsule is 1 mm. Each capsule contained approximately 40 mg of TLD powder. The TLD capsules utilized were ‘double loaded’; each capsule contained two discrete aliquots (allowing for more measurement points). The volume of each of these aliquots is approximately 13 mm³.

2.7.1 TLD Dose Calculation

The following formalism is utilized by the RPC for the calculation of dose from the thermoluminescent response of the TLD (Davidson 2006).

$$D = TL * S * K_l * K_f * K_e$$

D: Absorbed dose to muscle

TL: Mean thermoluminescent response per unit mass

- S: Sensitivity or absorbed dose per thermoluminescent response for standards irradiated with ^{60}Co
- K_l : Linearity correction
- K_f : Fading correction
- K_e : Correction to energy used to irradiate (6 MV)

Determination of S:

The sensitivity, S, was determined during each TLD readout session, and corrects for variations of the reflectivity of the planchette, optics, and electronics. First, TLD known as ‘high dose standards,’ were irradiated in ^{60}Co to approximately 20 Gy. Six high dose standards were read, three at the beginning of the session, three at the end of the session. The following equation was used to calculate S for the session:

$$S = \frac{D_s}{K_l * K_f * T_s}$$

- D_s : Expected dose to TLD (decay corrected ion chamber measurement)
- T_s : mean thermoluminescent response for the high dose standards per unit mass
- K_l : Linearity correction
- K_f : Fading correction

Determination of K_l :

The linearity correction, K_l , corrected the supra-linearity of the thermoluminescent response (TL). For a batch of TLD (in this case, ‘B07’), capsules were irradiated to ten dose levels, varying from 3-50 Gy. Three capsules were averaged

at each dose level. This mean TL signal was then corrected for sensitivity and fading, and normalized to the TL signal at the 3 Gy level. This normalized dose response was then plotted against the relative signal. The inverse of this plot was calculated and fit with a second order polynomial. This resultant relationship follows:

$$K_l = aD_l^2 + bD_l + c$$

$$a = 2.290\text{E-}08$$

$$b = -2.12\text{E-}04$$

$$c = 1.06$$

$$D_l = \text{TL} \cdot S \cdot K_f \cdot K_e$$

Determination of K_f :

The TL response is dependent upon the time elapsed between the irradiation of TLD and the readout. To correct for dependence, the fading of a batch B07 was characterized with a double exponential:

$$K_f = \frac{N}{Ae^{-Bd} + Ce^{-Dd}}$$

$$d = \text{number of days elapsed between irradiation and readout}$$

$$N = 1.35$$

$$A = 1.28$$

$$B = 1.08\text{E-}4$$

$$C = 0.068$$

$$D = 0.072$$

Determination of K_e :

The energy correction was calculated as the ratio of the response of TLD for ^{60}Co energy to the response of TLD at the energy of interest; for these trials, the energy utilized was 6 MV. The correction applied for TLD irradiated at this energy was 1.03.

The TLD from each phantom irradiation trial were read by RPC staff members. The results from the reading session include TL reading from controls and high dose standards used to calculate the system sensitivity; dates and times for irradiations are also included for fading corrections. These data were used in a TLD dose calculation spreadsheet which iterated the solution to the previously described formalism to find the absorbed dose to TLD.

2.7.2 Film Dosimetry

The radiochromic film measured the relative dose distributions. The optical density of the film changes as a function of the dose received (due to a radiation induced polymerization within the active layer of the film). The film was calibrated according to RPC protocol. A piece of film from the batch being utilized for the irradiation trials was cut into 3 cm by 3 cm squares. These calibration films were placed under 1.5 cm of solid water with a further 9 cm of solid water as backscatter material. The calibration films were then irradiated progressively from 50 monitor units to 1350 monitor units at a field size of 35 cm by 35 cm. This process was repeated three times.

The calibration films were scanned using the RPC's film scanner, a CCD100 Microdensitometer manufactured by the Photoelectron Corporation (North Billerica, MA). The scanned films were exported as 32 bit .FIT files.

The films were analyzed in ImageJ. ImageJ is open source image analysis software developed by Wayne Rasband of the Research Services Branch of the NIH (Bethesda, MD). At each irradiation level, the mean optical density of the calibration film was measured. The mean optical density was averaged across the three trials at each irradiation level. The MUs delivered were converted to dose at the film depth by multiplying by the output factor at a 35 cm x 35 cm field size. The film was at D_{\max} for the unit used, so no percent depth dose correction was needed.

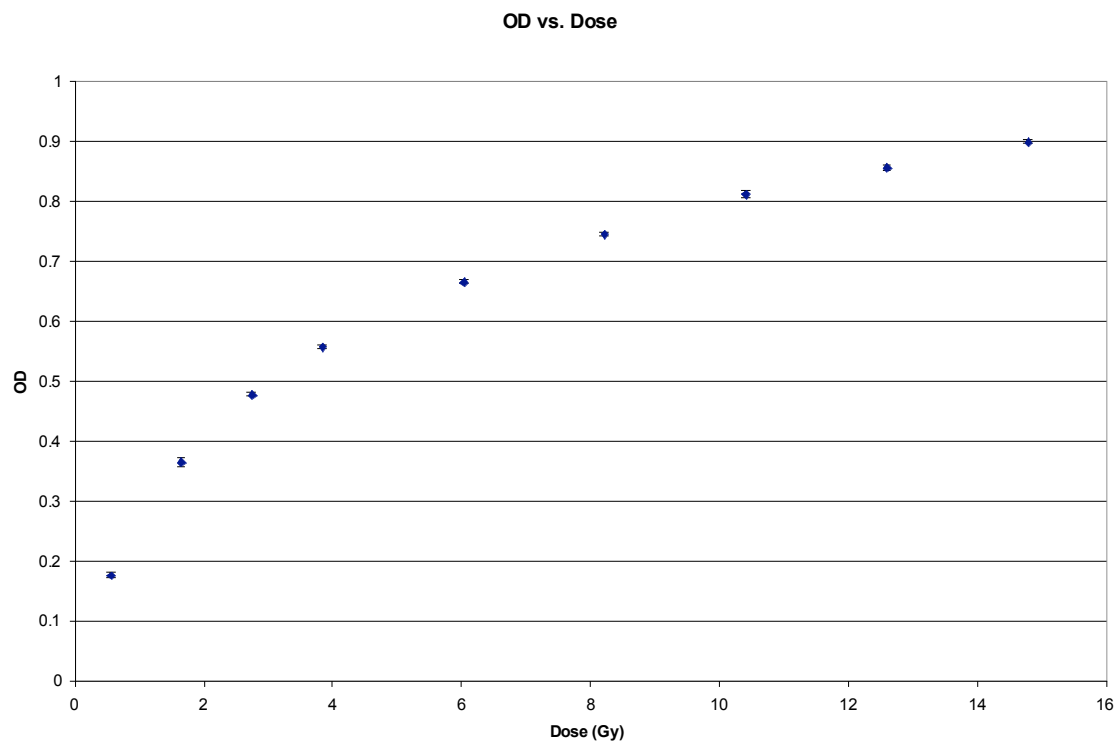


Figure 2.13: The dose response curve for the batch of Gafchromic EBT film utilized in this study; the chart plots the optical density against the dose.

The function to calculate the dose from a measured optical density was calculated by inverting the data, and fitting a cubic function to the dose vs. OD curve, per RPC protocol. The function calculated was as follows, with an R^2 of .99:

$$Dose(OD) = 29.38 \cdot OD^3 - 14.96 \cdot OD^2 + 5.92 \cdot OD$$

This dose response curve, shown in figure 2.13, was not used for absolute dosimetry; rather, it was used to measure the relative dose distribution. The measured distributions were corrected by the measured TLD dose.

2.7.3 Radiochromic Film Data Collection and Calibration to TLD

Using the CCD100 film scanner, the film results from each phantom irradiation trial were converted into .FIT files, which contained a 512 by 512 array of the OD values. These files were read into MATLAB and were converted to dose (cGy) using the cubic fit from the dose response curve. These values were then converted to 16 bit .TIF image files, with each pixel value in cGy. Thus, the minimal step was 1 cGy, and the typical range recorded on the film was up to 1400 cGy.

The film was then corrected to the measured TLD dose. For each trial, there were four TLD measurements: Anterior/Superior, Anterior/Inferior, Posterior/Superior, and Posterior/Inferior. On the axial film, the mean doses at the two small circular localities where the TLDs abut the film were measured. The ratio of the TLD dose to the film dose was calculated (at each location). The average of these ratios was calculated. The film response was then multiplied by this ratio. For the sagittal films, the same principle was used, but the mean was taken of a rectangular region running the length of the TLDs.

Figures 2.14 and 2.15 show the position of the TLDs relative to the calibration areas on the film.

After the conversion to dose and the correction to the TLD dose measurement, the film was registered to the planned dose distribution for gamma analysis.

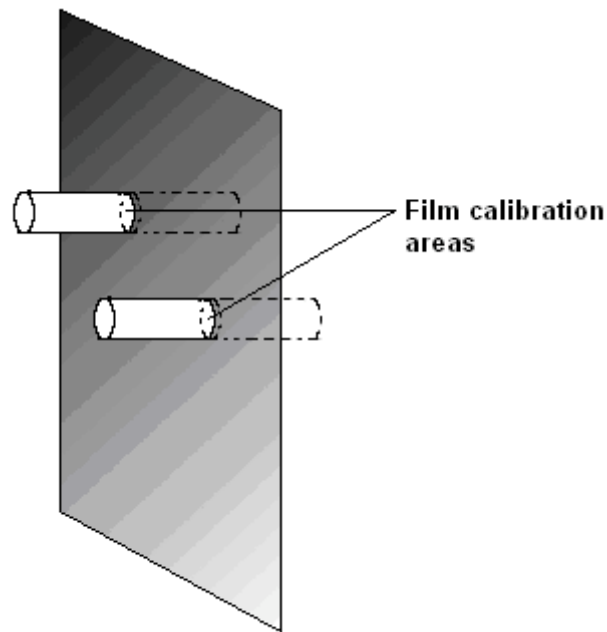


Figure 2.14: An illustration of the calibration points of the film relative to the TLDs for the axial plane.

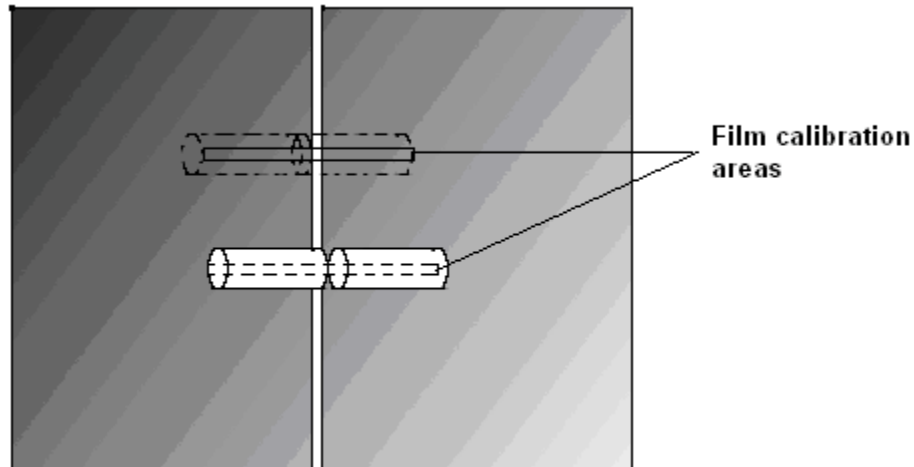


Figure 2.15: *An illustration of the calibration points of the film relative to the TLDs for the sagittal plane.*

2.7.4 Exporting Dose Planes from the TPS

The ‘dose plane’ functionality within the Pinnacle TPS allows the user to sample an arbitrary 2-D distribution from the dose volume. The physical film planes were visible on the CT image in the planning interface of the Pinnacle software, which allowed for an accurate selection of the correct plane for comparison. After calculation of the dose distributions on a $2 \times 2 \times 2 \text{ mm}^3$ dose grid, the dose was interpolated to $1 \times 1 \text{ mm}^2$ pixels. These planes were exported from Pinnacle, and reformatted into 16 bit .TIF images, with each pixel value in cGy.

2.7.5 Processing and Registration of Measured Data

The pin pricks on the film provided the registration points to the planned dose. The pin pricks were visible on the 16-bit TIF film images. However, the pin prick locations had to be added to the 16-bit TIF planned dose distributions; this was accomplished through an overlaying process. The planned dose distributions, in a given

plane, were collimated to a known size. The CT image was then collimated to the same size. The CT image was overlaid onto the dose distribution, and the pin-prick locations were ‘burned’ (by changing the dose value at those points) into the planned distribution. This process was conducted for each planned dose distribution.

Both the planned and measured distributions then had registration marks. However, there were differences in scaling and rotation between the images. To address this, the coordinates of the pin pricks on the measured and planned distributions were found in ImageJ. Then, image processing functionalities within MATLAB were used to calculate a transformation matrix between these sets of points. The underlying distortion between the images were rotation and scaling, so a ‘linear conformal’ transformation matrix was calculated. For scaling the measured dose distribution, a bilinear interpolation was utilized, per the procedure described by Childress et al. for conducting gamma analyses (Childress 2005). Also, a smoothing median filter was applied to the measured distribution to reduce noise, per RPC protocol (Davidson 2006). The transformation matrix was applied to the measured dose distribution. The result is a smoothed image scaled and rotated for an exact pinprick overlay to the planned distribution; this process downsampled the measured distribution to meet the resolution constraint of the planned dose distribution. This process, shown in Figure 2.16 was conducted for each individual piece of film; one axial film per trial, and two sagittal films per trial.

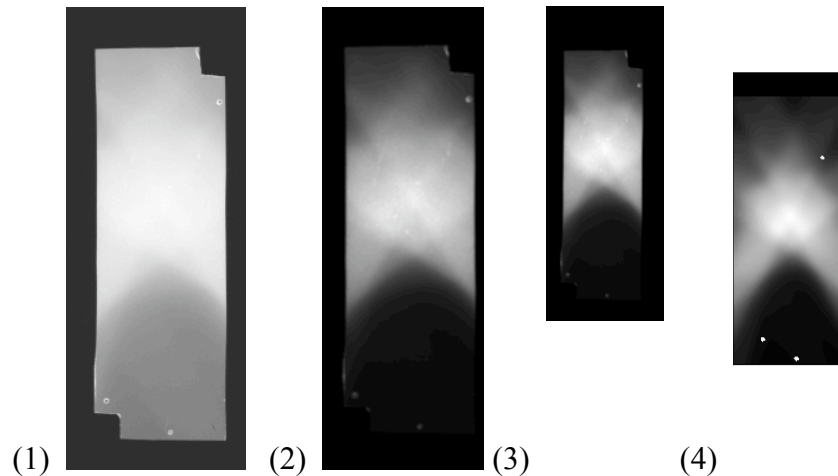


Figure 2.16: Data processing: (1) Raw OD data for one of the axial films from an irradiation trial. (2) OD data processed by the dose response curve and smoothed with a median filter. (3) The resultant dose distribution downsampled with bilinear interpolation and rotated to match the pin-prick locations of the planned distribution, shown in (4), with the pin locations ‘burned’ onto the image.

2.9 Data Analysis: Gamma calculations, Isodose Planes and Profiles

Once the films were registered, the data were then read into DoseLab, publicly available software for routine analysis of various dose distributions, created by Nathan Childress (Childress 2005). The software was used for gamma calculations between planned and measured distributions. Also, the software allowed for other qualitative assessments of the distributions. Along with each of the gamma calculations, the following assessments were included: isodose overlays, dose profiles, and point dose comparisons. These types of assessments are utilized by the RPC for dose comparison in a variety of IMRT phantom studies (Davidson 2006) (Molineu 2005). For the dose profiles, the 5% dose difference and 3 mm DTA criteria were built onto the measured film profiles by implementing the gamma calculation in one dimension in a Microsoft Excel spreadsheet (Low 1998).

2.9.1 Gamma Analysis

Gamma analysis has become a useful tool for routine IMRT quality assurance in clinics. Gamma analysis takes into account both distance-to-agreement (DTA) and dose difference in comparing planar dose distributions. Gamma analysis takes advantage of the complementary sensitivities of DTA and dose difference, which are sensitive to low and high dose gradients, respectively.

For two registered planar dose distributions, gamma analysis calculates the dose difference and DTA for each pixel as components of a vector normalized to the criteria of interest; if the magnitude of that vector exceeds 1, then that pixel fails the gamma analysis at the defined criteria (Low 1998).

In Fig. 1, (r_c, D_c) is a point on the calculated dose distribution (from treatment planning software), and (r_r, D_r) is a point on the reference dose distribution (measured from the film plane). The symbols Δd_M and ΔD_M are user defined tolerances for distance-to-agreement and dose difference, respectively.

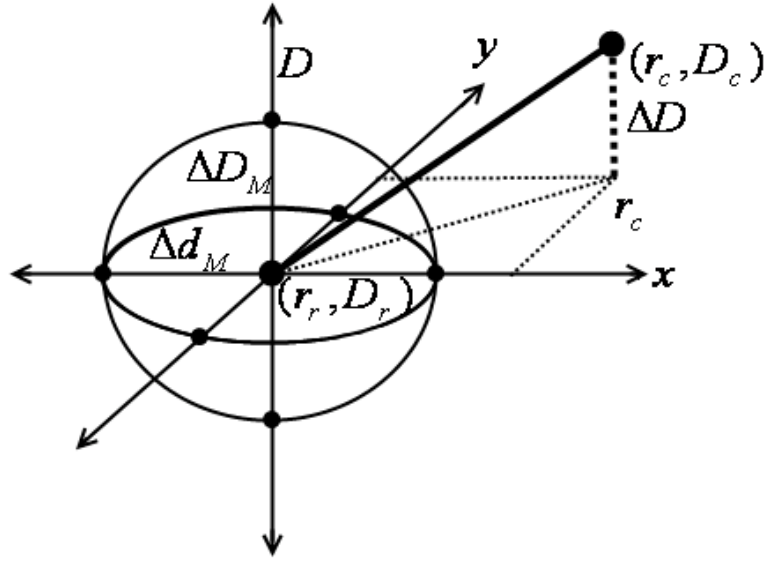


Figure 2.17: Geometric relation of points used for a 2-D gamma calculation in assessing the reference and calculated distributions. The x and y axes denote the spatial location of dose, and D denotes the dose axis, and (r_c, D_c) denotes an arbitrary calculated dose value and location.

The ellipsoid is defined on the reference distribution by the selected tolerances for Δd_M and ΔD_M . The calculated distribution is queried for the minimum gamma value, $\Gamma_r(r_c, D_c)$:

$$\Gamma_r(r_c, D_c) \equiv \sqrt{\frac{\Delta r^2}{\Delta d_M^2} + \frac{\Delta D^2}{\Delta D_M^2}}$$

where ΔD and Δr are defined as follows:

$$\Delta D = D_c - D_r$$

$$\Delta r = r_c - r_r$$

The γ value for a point on the reference distribution is the smallest value of $\Gamma_r(r_c, D_c)$ calculated. If the γ value is less than or equal to one, that point passes the criteria (Low 1998). The percentage of passing points across a distribution is used as a proxy for how well the planned and measured distributions accord.

2.9.2 Criteria Utilized

At what level should the tolerance for acceptable agreement between dose distributions be defined? For daily IMRT quality assurance regimens, a variety of tolerances are utilized in different clinics. For daily IMRT QA, M.D. Anderson utilizes a 5% dose difference and 3 mm distance to agreement; a dose distribution assessment fails if less than 80% of the pixels pass the gamma analysis (Childress 2005). The RPC utilized a range from 5% / 3mm to 7% / 7mm in assessing agreement of radiation therapy fractions to its lung phantom. Davidson et al. found greater than 95% pixel passing rates for the 5% / 3mm criteria when utilizing the collapsed-cone convolution dose algorithm with heterogeneity correction (Davidson 2006). For intensity modulated stereotactic body irradiations, UCLA conducts its quality assurance at a slightly tighter requirement, 3% / 3mm (Slotman 2006). The 3% / 3mm criteria were described as ‘quite stringent’ by the authors, and that small areas of disagreement are expected in a gamma analysis.

In this project, the dose agreement criteria were the 5% / 3mm criteria utilized by Davidson et al. The threshold for acceptable agreement used was a 95% pixel passing rate across a given dose plane. An assessment at tightened dose difference and DTA

criteria, 3% / 2mm, was conducted as well; these tighter criteria addressed the demand for high geometric and dosimetric accuracy for a radiosurgical procedure.

Chapter 3 Results and Discussion

3.1 Introduction

The following sections detail each of the parameters tested for each of the irradiation plans: TLD measurements, dose profiles, isodose curves, and gamma analyses. In each section, the results of each treatment plan are presented in this order: four-field box, conformal, IMRT plan #1, and IMRT plan #2. The four-field box irradiation had a simple geometry, and was used to establish a base line agreement for the non-modulated irradiation. Next, the conformal irradiation was assessed; this plan had no modulation, but had increased complexity in beam geometry. The four-field and conformal irradiations were not clinically feasible plans. Next, IMRT plan #1 was assessed. IMRT plan #1 did not meet the dose constraint requirements set forth by RTOG Protocol 0631. Also, this plan was administered incorrectly (with an approximately 2.5 mm shift from isocenter). These results are presented to demonstrate how a misadministration appears in the analysis. According to Andrea Molineu, an RPC physicist, about 15% of institutional failures in irradiating RPC phantoms are attributed to improper localizations, so the data from the IMRT plan #1 could help establish how an improper localization appears in the spine phantom. Finally, IMRT plan #2 was analyzed. IMRT #2 is an optimized plan and satisfied the clinical guidelines set forth in RTOG Protocol 0631.

3.2 Qualitative Assessment of Anatomic Utility

There is no ‘perfect’ spinal tumor patient on which to base a phantom model; these tumors present in a wide range of sizes and anatomical locations. Institutions have utilized a variety of solutions for spine phantoms in spinal radiosurgery quality assurance.

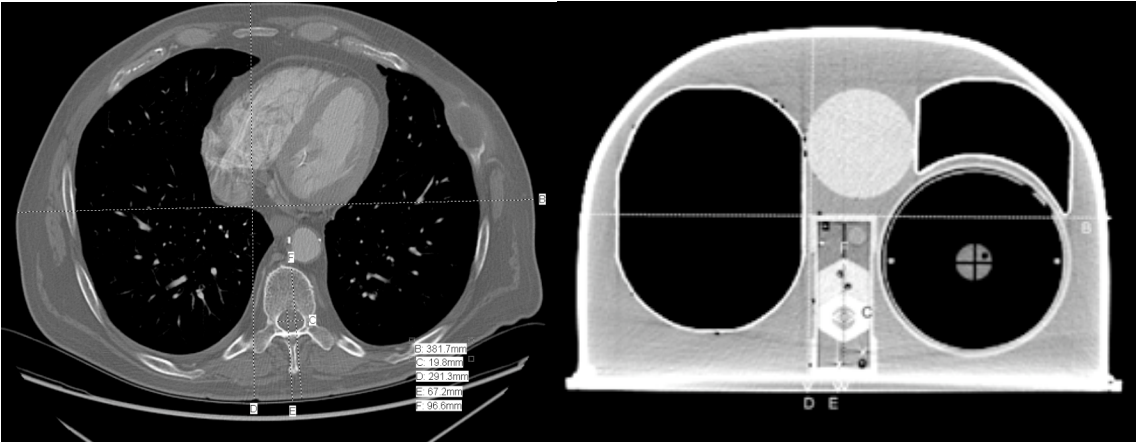
Yin et al. utilized a Rando® phantom (with simulated bone and lungs) loaded with radiochromic film and an ion chamber for validation study of its spinal radiosurgery treatments (Yin 2002). Medin et al. remapped treatment plans onto a CIRS thorax phantom (with simulated lungs) for patient specific quality assurance (Medin 2006). The spine phantom studied here was designed with the unique needs of the RPC in mind; compromises were necessary to produce a phantom that is durable, water-filled, anatomically simple and relatively inexpensive to produce. Thus, anatomical features were approximated with geometric shapes. A few other considerations were made for the spine phantom to be a representative spinal tumor case and a useful tool for the RPC: location, depth, and size of the target volume.

Among 30 patients with spinal metastases treated by Dodd et al., the most frequent disease site was the thoracic vertebral body, which is where the target volume for the spine phantom is located (Dodd 2008).

Patients with spinal metastases at the University of Pittsburgh Medical Center (Pittsburgh, PA) and Henry Ford Hospital (Detroit, MI) have their entire vertebral body and pedicles of the involved site delineated as the target volume (Ryu 2009). In the spine phantom, the design of the target volume shape approximated a vertebral body with pedicles.

The depth and size of the target volume (the vertebral body and pedicles) in the spine phantom should be close to that of a patient with a chest of similar breadth. CT scans of a male M.D. Anderson patient were selected for comparison; this patient had a chest breadth similar to that of the spine phantom. A side-by-side comparison between the spine phantom and this patient demonstrated similarities in the proportion of the

phantom anatomy to that of the patient. The comparison relied primarily on an axial view of the patient at the level of the heart, where the pedicles clearly define the spinal canal.



Distance Comparison <i>Anatomy Measured:</i>	Distance (cm)	
	<i>Patient</i>	<i>Phantom</i>
<i>Left to Right</i>	38.2	36.3
<i>Anterior to Posterior</i>	29.1	25
<i>Posterior to Anterior of Spinal Canal</i>	6.8	6.7
<i>Posterior to Anterior of Vertebral Body</i>	9.7	9.1
<i>Diameter Spinal Canal</i>	2.0	1.5
<i>Thickness of Vertebral Body (not shown)</i>	3.4	5.0

Figure 3.1: A comparison of important anatomical distances between a male patient and the spine phantom.

The table in Figure 3.1 shows a close agreement for critical distances between the patient and the spine phantom. The depth of the tumor, the size of the spinal canal, and the size of the treatment area were similar in scale for the phantom and the patient. The thickness of the target volume of the spine phantom was slightly more than that of the vertebral body of the patient.

Another important aspect of the spine phantom is the relation of the tumor to the spinal canal. RTOG 0631 does not allow patients to enter the protocol when a lesion is

closer than 3 mm to the spinal cord (RTOG 2009). In the phantom, the shortest distance between the spinal canal and the target volume was approximately 7 mm.

The target volume in the spine phantom was measured to be 41.5 cm³. After 500 cases at their institution, Gerszten et al. found an average tumor volume of 46 cm³, with a range of volumes from 0.2 cm³ to 264 cm³. The tumor volume for the spine phantom is near the average case, appropriate as a representative case (Gerszten 2007).

3.3 TLD Measurements

Tables 3.1-3.4 and figures 3.2-3.5 show the absolute dose measurements at each of the TLD locations within the target volume. They were labeled as Anterior/Superior, Anterior/Inferior, Posterior/Superior, Posterior/Inferior; the relative locations are shown in Figure 2.4 in the Methods and Materials section. In each TLD capsule were two separate aliquots of powder. Each of these aliquots contributed a single measurement. Because of the close spatial proximity of these aliquots, they were grouped together. Thus, over three irradiations, each TLD location had 6 samples. The planned dose to each point was calculated by measuring the average dose to the TLD contour in the TPS. The coefficient of variance was also calculated for each TLD location, so that the relative spread could be compared between points.

3.3.1 Four-Field Box: TLD Results

Table 3.1 shows the TLD results from the four-field box irradiation.

4-Field Box					
-------------	--	--	--	--	--

<i>TLD Position:</i>	<i>Mean Dose (cGy)</i>	<i>Sample S.D.</i>	<i>COV (%)</i>	<i>Planned Dose (cGy)</i>	<i>Planned/ Measured</i>
<i>Superior/Anterior</i>	900.8	7.3	0.8	898.0	0.997
<i>Inferior/Anterior</i>	904.0	6.6	0.7	906.3	1.003
<i>Superior/Posterior</i>	921.4	9.7	1.1	908.3	0.990
<i>Inferior/Posterior</i>	909.6	13.0	1.4	908.8	0.999

Table 3.1: The absorbed dose to TLD at each position for the Four- Field Box irradiation. The sample standard deviation and COV (%) was calculated at each point. The ratio of planned/measured was calculated for each TLD position.

In order to show the agreement between the measured and planned dose for each TLD location, Figure 3.1 shows the ratio of the planned to measured data with error bars indicating the 95% confidence interval at each location (n = 6 measurements) for the four-field box irradiation.

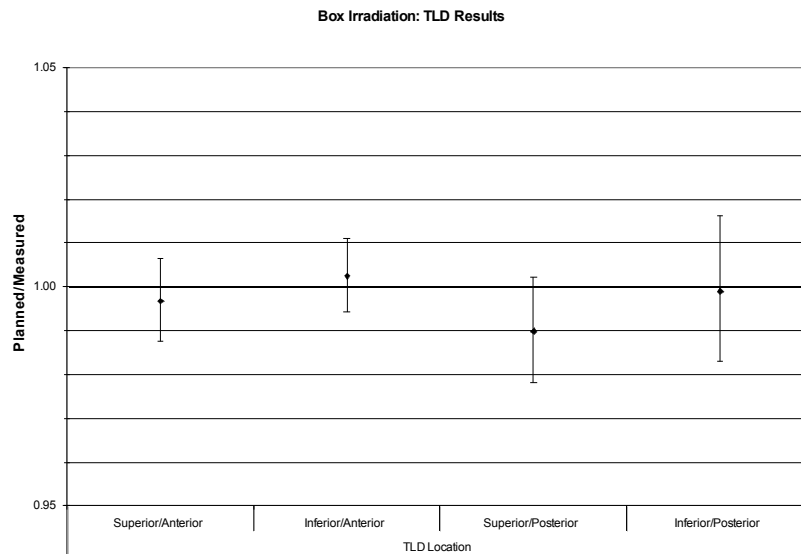


Figure 3.2: The ratio of the planned to measured dose for the Four-Field Box irradiation with 95% C.I.'s for n=6 measurements. Each gridline indicates a 1% change, and the gridline at a ratio of 1 is in bold.

Figure 3.1 demonstrates that the TLD measurements agree well with the planned dose. The mean dose measured is slightly more than 1% off at the Superior/Posterior location. At each location, the null hypothesis that Planned/Measured = 1 was tested at the 5% confidence level. At each TLD location, the null hypothesis was not rejected.

3.3.2 Conformal Irradiation: TLD Results

Table 3.2 shows the TLD results from the conformal irradiation with the standard deviation, COV (%), and the ratio of planned to measured dose.

Conformal					
<i>TLD Position:</i>	<i>Mean Dose (cGy)</i>	<i>Sample S.D.</i>	<i>COV (%)</i>	<i>Planned Dose (cGy)</i>	<i>Planned/ Measured</i>
Superior/Anterior	919.3	6.1	0.7	920	1.001
Inferior/Anterior	928.9	7.5	0.8	927.2	0.998
Superior/Posterior	959.1	9.0	0.9	960.1	1.001
Inferior/Posterior	957.3	10.6	1.1	961.8	1.005

Table 3.2: The absorbed dose to TLD at each position for the Conformal irradiation.

The sample standard deviation and COV (%) was calculated at each point. The ratio of planned/measured was calculated for each TLD position.

The following figure shows the ratio of planned to measured dose at each TLD location for the conformal irradiation. The 95% C.I.'s are shown for each point.

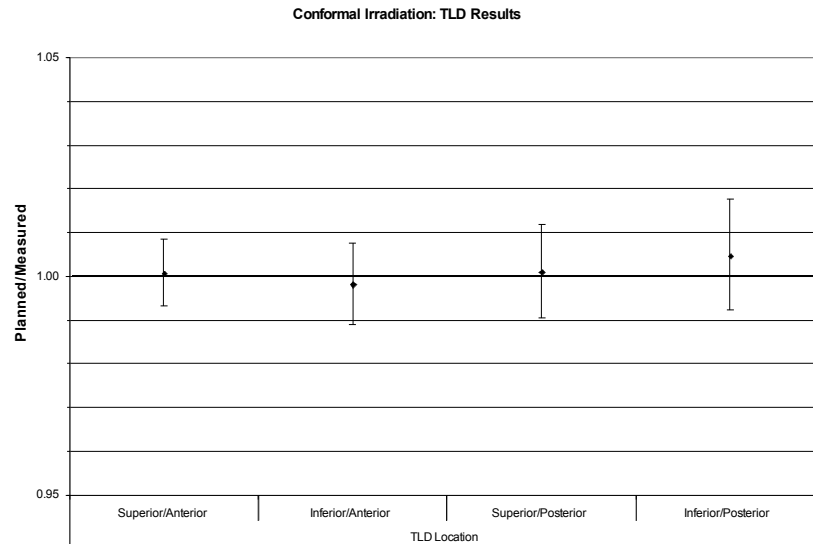


Figure 3.3: The ratio of the planned to measured dose with 95% C.I.'s for $n=6$ measurements. Each gridline indicates a 1% change, and the gridline at a ratio of 1 is in bold.

Figure 3.2 shows good agreement between the measured dose and the planned dose for the conformal irradiation. At each location, the null hypothesis that $\text{Planned/Measured} = 1$ was tested at the 5% confidence level. At each TLD location, the null hypothesis was not rejected.

3.3.3 IMRT #1: TLD Results

The following table shows the TLD results from the conformal irradiation with the standard deviation, COV, and the ratio of planned to measured dose.

IMRT #1					
TLD Position:	Mean Dose (cGy)	Sample S.D.	COV (%)	Planned Dose (cGy)	Planned/Measured
Superior/Anterior	830	10.5	1.3	863	1.040
Inferior/Anterior	807.2	4.7	0.6	857.9	1.063
Superior/Posterior	795.7	8.0	1	843.6	1.060
Inferior/Posterior	787.1	17.2	2.1	833.2	1.059

Table 3.3: The absorbed dose to TLD at each position for each trial for the IMRT #1 irradiation. The sample standard deviation and COV (%) was calculated at each point. The ratio of planned/measured was calculated for each TLD position.

The following figure shows the ratio of planned to measured dose at each TLD location for the conformal irradiation. The 95% C.I.'s are shown for each point.

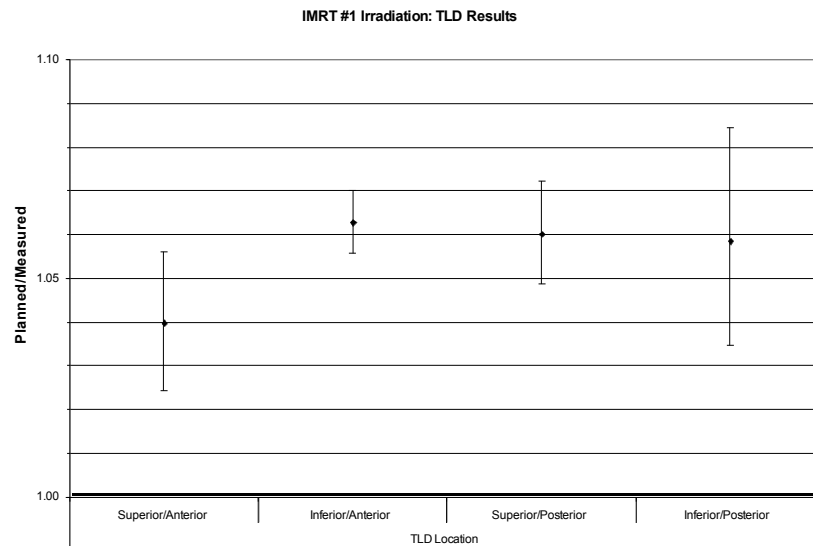


Figure 3.4: The ratio of the planned to measured dose with 95% C.I.'s for $n=6$ measurements. Each gridline indicates a 1% change, and the gridline at a ratio of 1 is in bold.

Figure 3.3 shows poor agreement between the mean dose to TLD and the planned dose for the IMRT plan #1 irradiation. However, this trial was misadministered (was

incorrectly localized by approximately 2.5 mm), and a difference in the measured and planned was expected, especially due to the large dose gradients within the target volume. The incorrect positioning was more apparent in the isodose distribution of these irradiations, shown in section 3.4.3. The method used to detect and measure the misadministration is also discussed in section 3.4.3. At each location, the null hypothesis that Planned/Measured = 1 was tested at the 5% confidence level. At each TLD location, the null hypothesis was rejected.

3.3.4 IMRT #2: TLD Results

The following table shows the TLD results from the conformal irradiation with the standard deviation, COV, and the ratio of planned to measured dose.

IMRT #2					
<i>TLD Position:</i>	<i>Mean Dose (cGy)</i>	<i>Sample S.D.</i>	<i>COV (%)</i>	<i>Planned Dose (cGy)</i>	<i>Planned/Measured</i>
Superior/Anterior	1059.1	14.0	1.3	1054	0.995
Inferior/Anterior	1050.7	20.0	1.9	1070	1.018
Superior/Posterior	1081	33.2	3.1	1083	1.002
Inferior/Posterior	1095.6	27.4	2.5	1092	0.997

Table 3.4: *The absorbed dose to TLD at each position for each trial for the IMRT #2 irradiation. The sample standard deviation and COV (%) was calculated at each point. The ratio of planned/measured was calculated for each TLD position.*

The following figure shows the ratio of planned to measured dose at each TLD location for the conformal irradiation. The 95% C.I.'s are shown for each point.

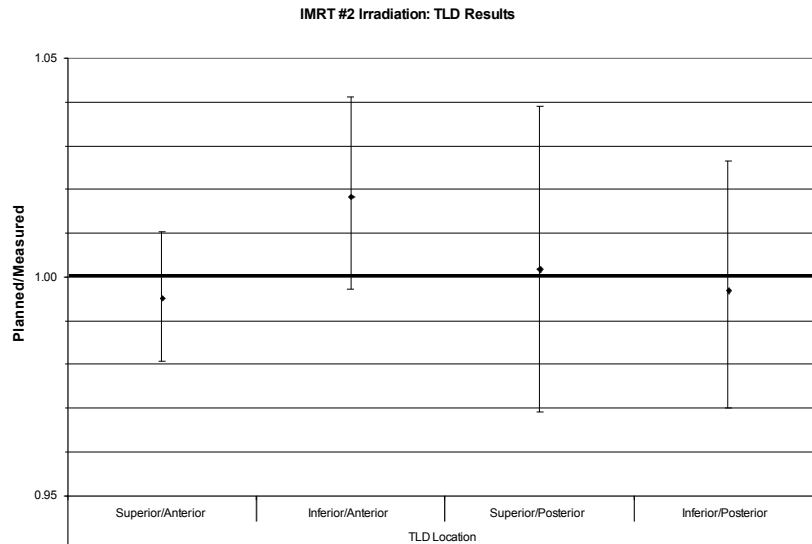


Figure 3.5: The ratio of the planned to measured dose with 95% C.I. 's for $n=6$ measurements. Each gridline indicates a 1% change, and the gridline at a ratio of 1 is highlighted.

Figure 3.4 shows good agreement between the mean dose to TLD and the planned dose for the IMRT plan #2 irradiation. However, at some locations, the 95% CI exceeded $\pm 5\%$. At each location, the null hypothesis that $\text{Planned/Measured} = 1$ was tested at the 5% confidence level. At each TLD location, the null hypothesis was not rejected. However, the 95% CI's were larger for the IMRT #2 irradiation than for the four-field box and conformal irradiations. This was likely due to the high dose gradients within the target volume and across the TLD themselves.

The mean dose measurement at each TLD location for the four-field box, conformal, and IMRT #2 plans were all within 2% of the planned dose. These results are consistent with TLD results of the RPC study by Davidson et al. that utilized a Pinnacle dose engine to predict dose in a lung phantom. In Davidson et al.'s study, the TLD dose

measurements were within 2% of the predicted measurement in three trials (Davidson 2006). These results are also well within the 5% dose difference criteria applied in the gamma analysis. These results demonstrated that, for a well-localized irradiation, the Pinnacle collapsed-cone convolution superposition dose engine accurately predicted the dose measured with TLD. One potential issue, however, is the steep dose gradients across the TLD; the size of the 95% confidence intervals indicate that there is greater uncertainty in intensity modulated irradiations such as IMRT plans #1 and #2 than in the four-field box and conformal irradiations. The standard deviation of the dose to the TLD contour, measured in the TPS, reveals a greater variation of dose across the TLD in the intensity modulated plans. Whereas the coefficients of variance of the mean dose to the TLD for the four field box and conformal plans are below 1%, the coefficients of variance of the mean dose to the TLD for the IMRT plans #1 and #2 are between 2% and 3%. This observation agrees with the greater uncertainties seen in the measured TLD doses of the intensity modulated plans.

3.4 Axial Profile and Isodose Distributions

Each sagittal and axial film plane was corrected to the TLD dose according to the procedure described Section 2.8.3. The planned and measured dose distributions were compared visually with isodose distributions and axial profiles. These comparisons provided context for the gamma analyses. The isodose distributions allowed for inspection of the agreement of selected dose contours across the entire film plane. Although only one dimension is assessed with the dose profile, the 5% / 3 mm was

displayed alongside. With the criteria displayed on the chart, the agreement of the planned and measured dose profiles was assessed relative to the 5% / 3 mm criteria.

For each irradiation, the axial dose profile was taken through a registration pinprick, as shown in Fig 3.6. For each measured dose profile, the three trials per irradiation technique were averaged.

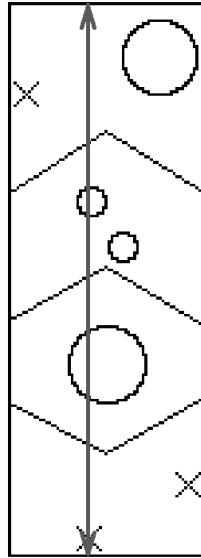


Figure 3.6: *The axial dose profile location: for each irradiation technique, the dose profiles were taken along the line indicated in the figure. The profiles were taken through the pinprick in order to register each of the film series together. For each irradiation technique, the 3 trials were averaged.*

3.4.1 Four-Field Box Plan: Isodose Distributions and Axial Dose Profile

Figure 3.7 shows the isodose distributions in the axial and sagittal planes of the first trial of the four-field box irradiation. The isodose distributions for the second and third trials are in the appendix.

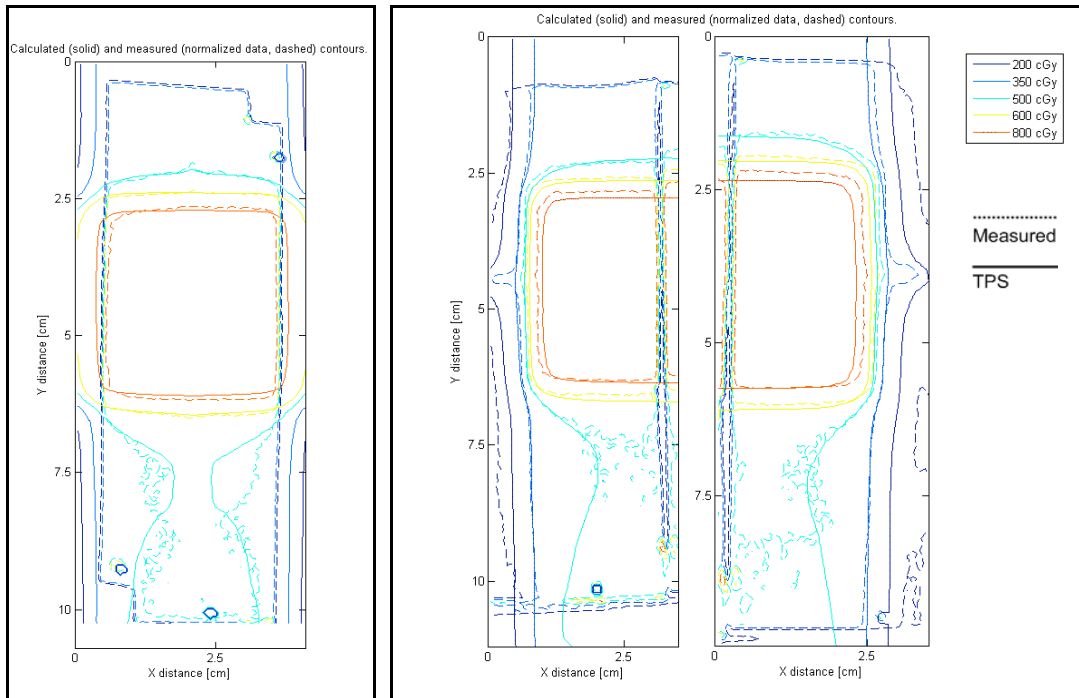


Figure 3.7: Isodose distributions for the axial and sagittal planes of the Four-field Box irradiation. The figure shows, from left to right, the axial, inferior sagittal, and superior sagittal planes. Due to small deviations in the cropping and registration, the scale is not the same for each portion of the figure.

Figure 3.7 visually demonstrates the close agreement of the selected isodose lines of the planned and measured dose distributions for the first trial of the four-field box irradiation. Because of some slight differences in registration of the superior and inferior portions of the sagittal film, there is some overlap of the display.

Figure 3.8 shows the mean axial dose profile and the planned dose profile.

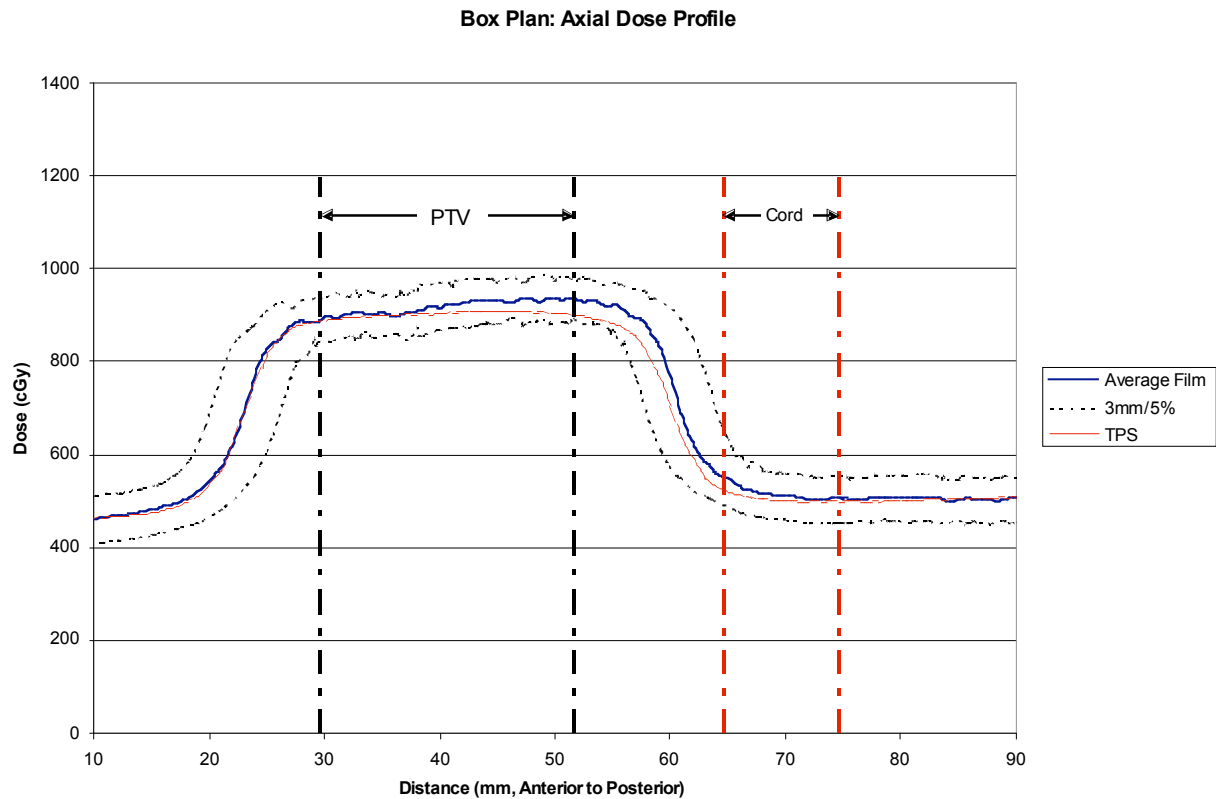


Figure 3.8: Axial dose profile: four-field box irradiation. The x-axis is the distance from the top of the cropped axial plane. The film dose profile is the average of the three trials. The 5% / 3 mm gamma criteria are represented as the dotted lines above and below the film dose profile. The planned tumor volume and spinal cord are also shown on the profiles.

Visual inspection of the graph of the planned to measured dose shows good agreement along the profile; the planned dose did not move outside of the allowed tolerance along the profile. However, the planned dose does deviate from the measured dose at the posterior surface of the PTV, but not by more than 5%.

For the four-field box irradiation, the planned and measured dose distributions agree across the film plane.

3.4.2 Conformal Plan: Isodose Distributions and Axial Dose Profiles

Figure 3.9 shows the axial and sagittal isodose distributions for the first trial of the conformal irradiation.

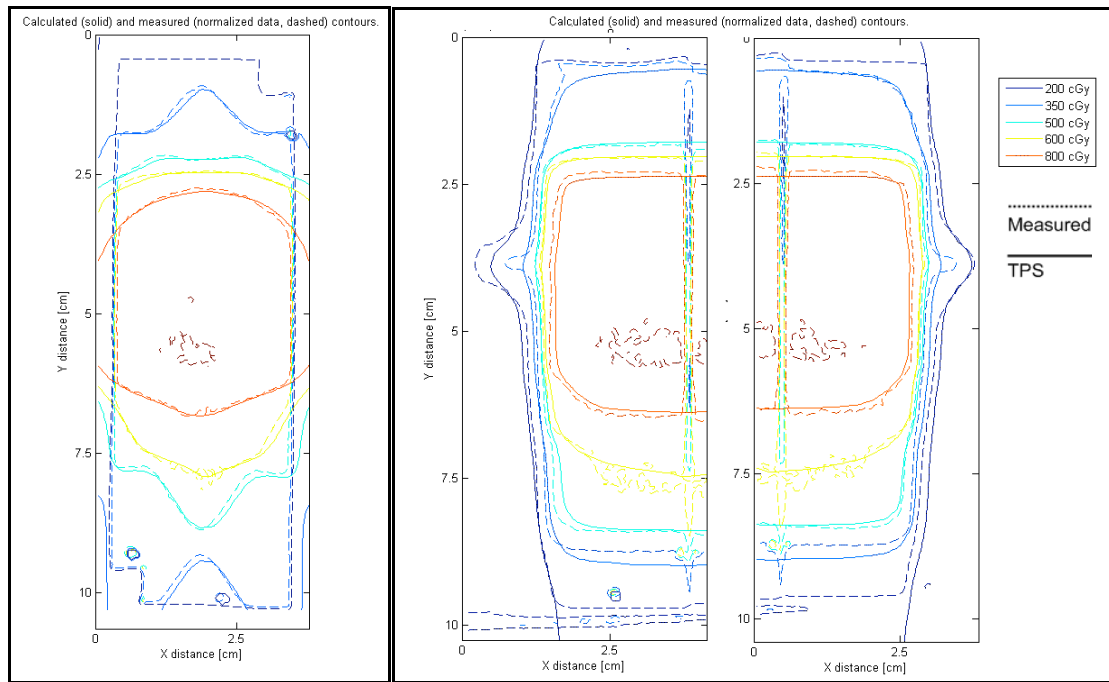


Figure 3.9: Isodose distributions for the axial and sagittal planes of the conformal irradiation. The figure shows, from left to right, the axial, inferior sagittal, and superior sagittal planes. Due to small deviations in the cropping and registration, the scale is not the same for each portion of the figure.

Figure 3.9 visually demonstrates the close agreement of the planned and measured dose distribution for the conformal irradiation. Small deviations of the planned dose from the measured are perceptible across the sagittal and axial film planes, but overall, there is a close agreement. Figure 3.10 is the axial dose profile for the conformal plan.

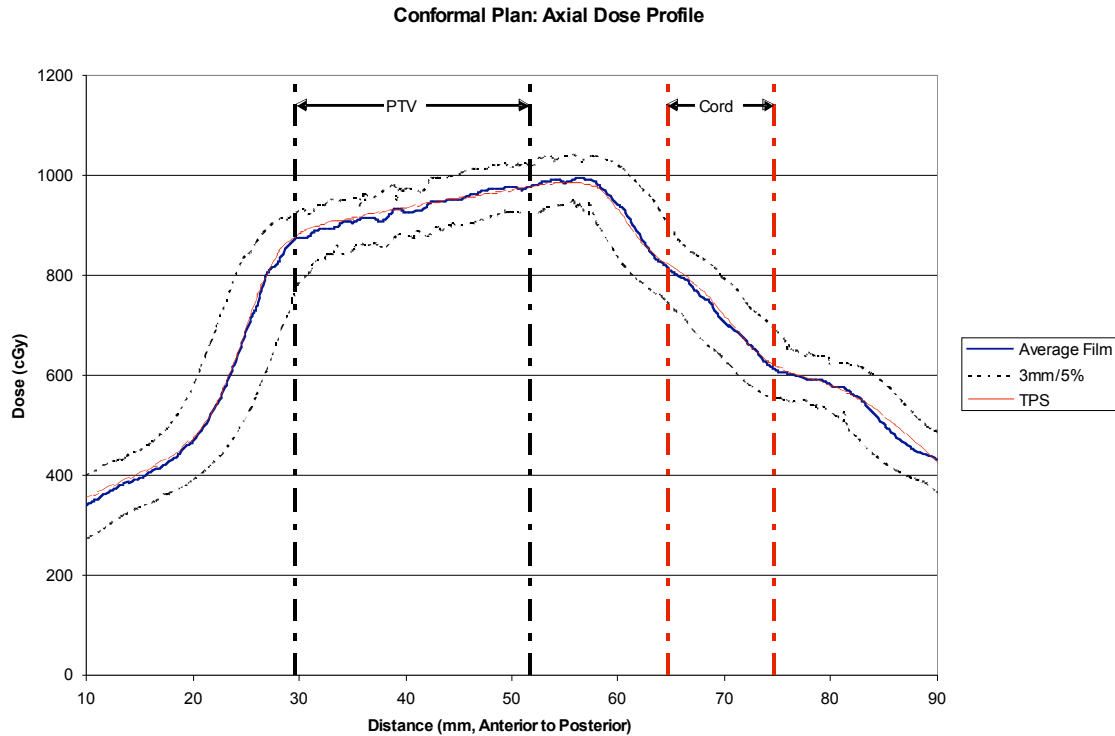


Figure 3.10: Axial dose profile: Conformal irradiation. The x-axis is the distance from the top of the cropped axial plane. The film dose profile is the average of the three trials. The 5% / 3 mm gamma criteria are represented as the dotted lines above and below the film dose profile. The planned tumor volume and spinal cord are also shown on the profiles.

In Figure 3.9, the axial dose profile demonstrates good agreement across the film plane. The planned dose is very close to the mean film dose (n=3 trials), and does not approach or exceed the 5% / 3 mm criteria bounding the measured dose.

3.4.3 IMRT #1 Plan: Isodose distributions and axial dose profile

Figure 3.11 shows the isodose distributions for the second trial of the IMRT #1 irradiation. The second trial is shown because the axial film of the first trial was over exposed (the film may have been exposed to fluorescent light).

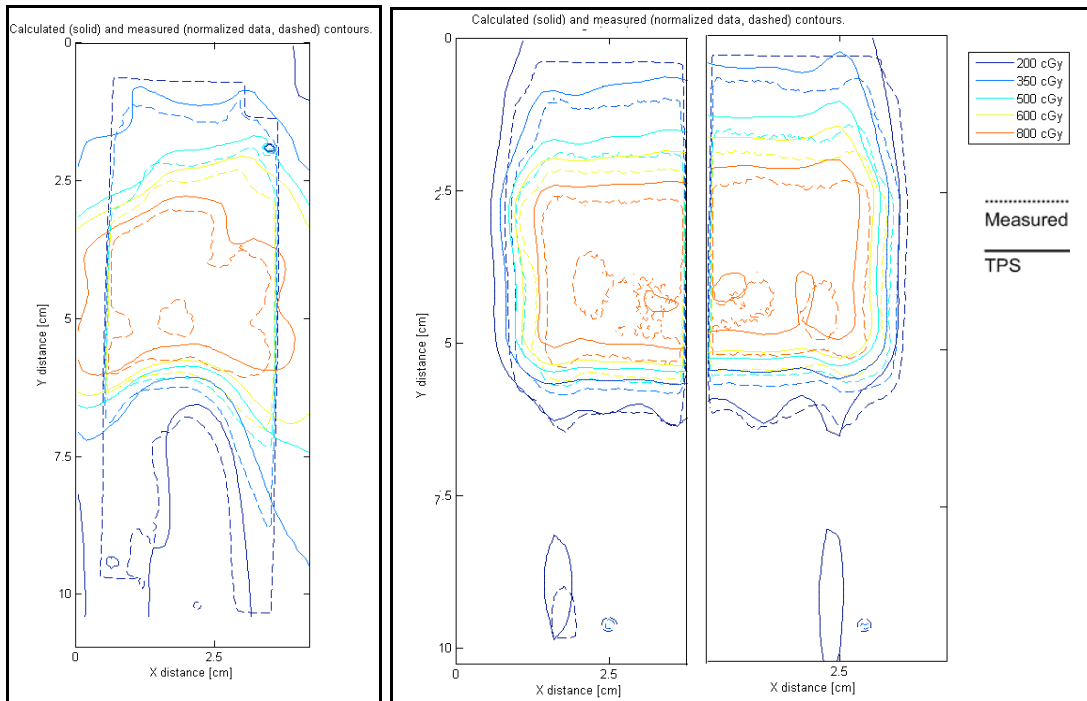


Figure 3.11: Isodose distributions for the axial and sagittal planes of the IMRT #1 irradiation. The figure shows, from left to right, the axial, inferior sagittal, and superior sagittal planes. Due to small deviations in the cropping and registration, the scale is not the same for each portion of the figure.

Figure 3.11 illustrates the result of the localization error during irradiation. The planned and measured distributions have similar forms, but the measured distribution is shifted relative to the planned distributions in 3 aspects: left, inferiorly, and posteriorly. The shift is approximately 2.5 mm in magnitude. This shift magnitude was calculated using the autocorrelation function in the DoseLab software; the software calculates a best fit between the planned and measured dose distributions, and the spatial shift from the pinprick registration to the calculated registration was measured. This error was expected, as the phantom was localized using external markers placed during simulation. Despite the localization error, the IMRT plan #1 data set was included to showcase how the error can be visualized using these modes of data presentation.

Figure 3.12 is the axial dose profile for the IMRT #1 irradiation.

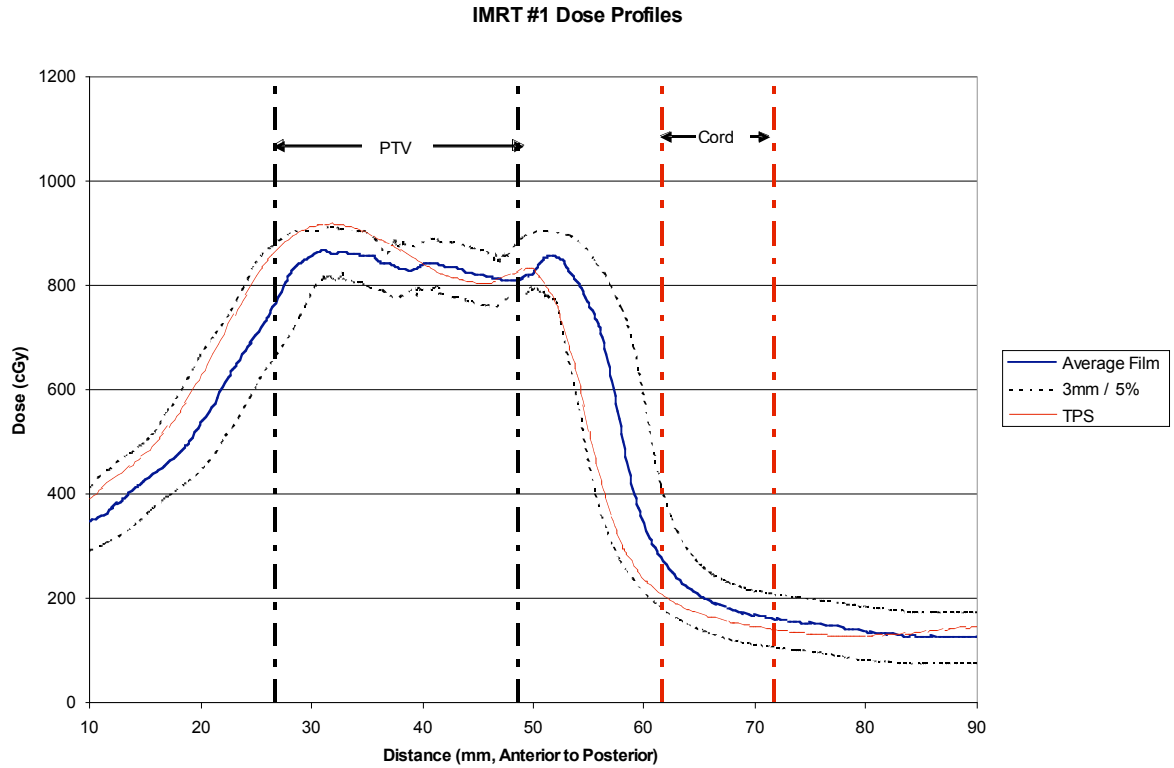


Figure 3.12: Axial dose profile: IMRT #1 irradiation. The x-axis is the distance from the top of the cropped axial plane. The film dose profile is the average of the two trials. The 5% / 3 mm gamma criteria are represented as the dotted lines above and below the film dose profile. The planned tumor volume and spinal cord are also shown on the profiles.

Again, the shift in the measured distribution relative to the planned distribution is apparent; while the profiles maintain the same form, the planned distribution nearly exceeds the dose difference and distance-to-agreement criteria along the profile, due to the localization error.

3.4.4 IMRT #2 Plan: Isodose distributions and axial dose profile

Figure 3.13 is the isodose distributions for the first trial of the IMRT plan #2 irradiation. The isodose distributions for the other trials are in the Appendix.

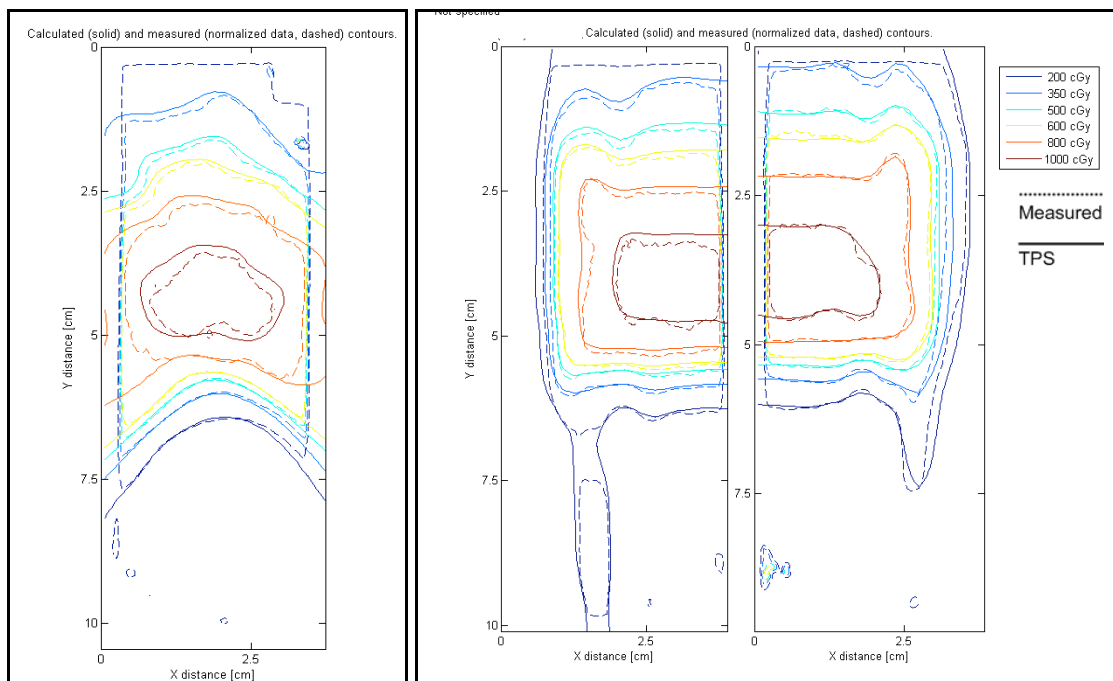


Figure 3.13: Isodose distributions for the axial and sagittal planes of the IMRT #2 irradiation. The figure shows, from left to right, the axial, inferior sagittal, and superior sagittal planes. Due to small deviations in the cropping and registration, the scale is not the same for each portion of the figure.

The isodose distributions for this trial demonstrate agreement between the planned and measured dose distributions. In the axial plane, the region of highest dose displayed (1000 cGy) is slightly smaller than the planned region. When scanning vertically down the sagittal and axial planes, the planned and measured isodose lines accord well along the steep dose gradient. The accordance along the steep dose gradient is demonstrated

with the axial dose profile, shown in Figure 3.14.

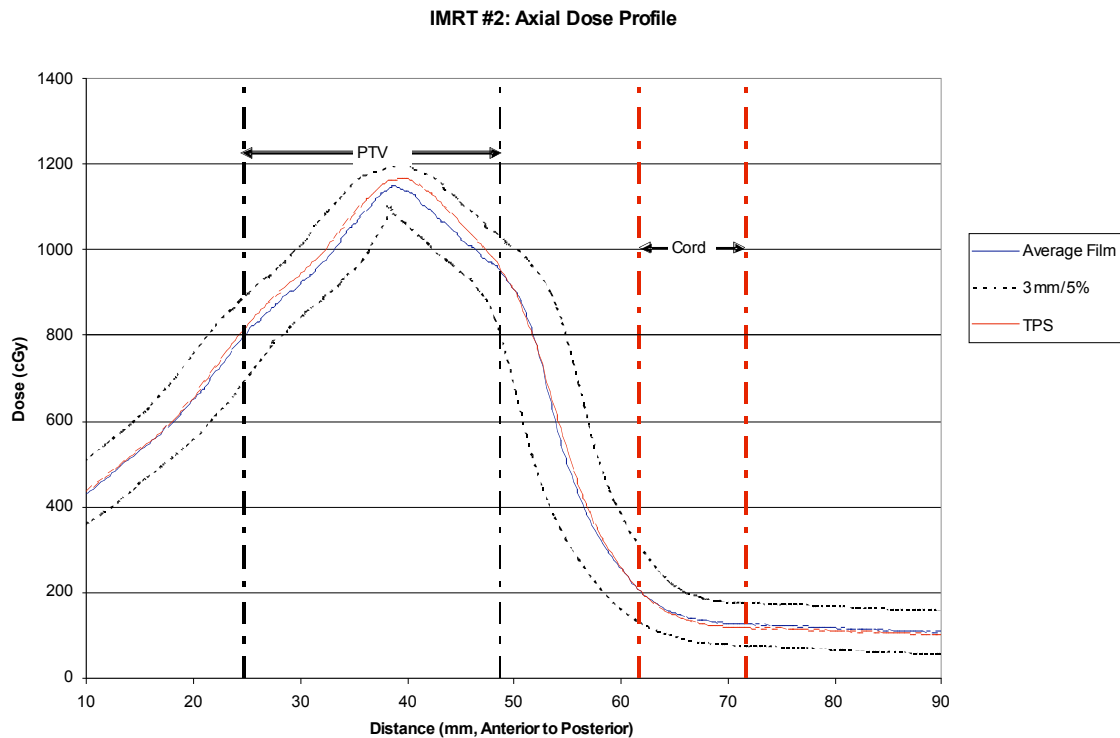


Figure 3.14: Axial dose profile: IMRT #2 irradiation. The x-axis is the distance from the top of the cropped axial plane. The film dose profile is the average of the three trials. The 5% / 3 mm gamma criteria are represented as the dotted lines above and below the film dose profile. The planned tumor volume and spinal cord are also shown on the profiles.

In Figure 3.14 the measured dose agrees well with the planned dose. The planned dose does not deviate much from the measured dose, and along the entire profile does not approach the bounding criteria. However, above 1000 cGy, the measured dose is slightly lower than the planned dose. This discrepancy is also apparent in the isodose distributions at 1000 cGy. These discrepancies may be attributable to the dose level selected for the prescriptions. The maximum dose in the PTV from IMRT plan #2 is significantly higher than the prescription dose of 800 cGy. Further scaling down the

prescription dose could allow for the film to capture the higher dose levels in a more useful portion of the dynamic range of the film where there is a greater change in the optical density per change in the dose.

3.5 Gamma Analysis

The gamma analyses were performed for the sagittal and axial film planes to test the accordance of the planned and measured distributions. The gamma analysis process is described in the Methods and Materials section; this project used the implementation in the publicly available DoseLab software. For each ‘gamma map’ presented in this paper, pixels on the gamma map passing the 5% / 3 mm criteria (gamma value less than 1) are shown in grayscale, while pixels with a value greater than or equal to 1 are color mapped from yellow to red, to clearly indicate where the gamma maps begins to fail to meet the criteria (Note: gamma values of 1 are considered passing, but are color mapped to enhance visualization of regions of failure). The axial and sagittal gamma maps for one trial of each irradiation are presented here (corresponding to the isodose distributions presented previously); the gamma maps for the remaining trials are in the Appendix. The following figures are the gamma maps for single trials for the four-field box, conformal, IMRT plan #1, and IMRT plan #2 irradiations.

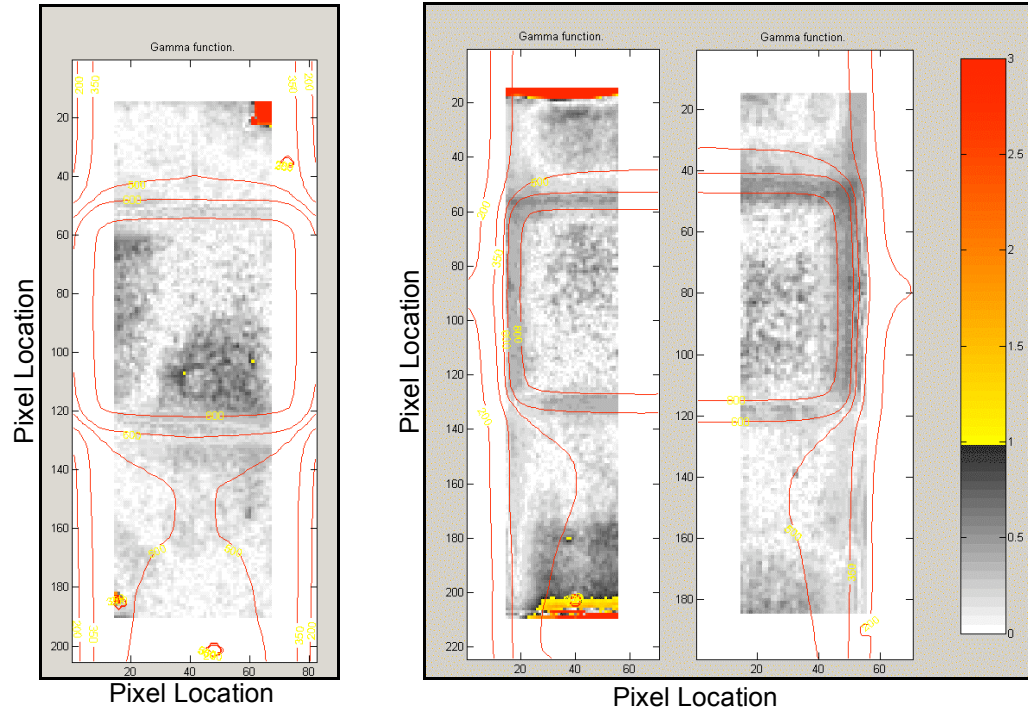


Figure 3.15: Gamma analysis maps of the axial and sagittal planes for the first trial of the Four-field Box irradiation. The x and y axes are the pixel locations. The gamma value at each point is color coded according to the bar on the right of the figure. Due to small deviations in the image cropping and registration, the scale is not exactly the same for each portion of the figure.

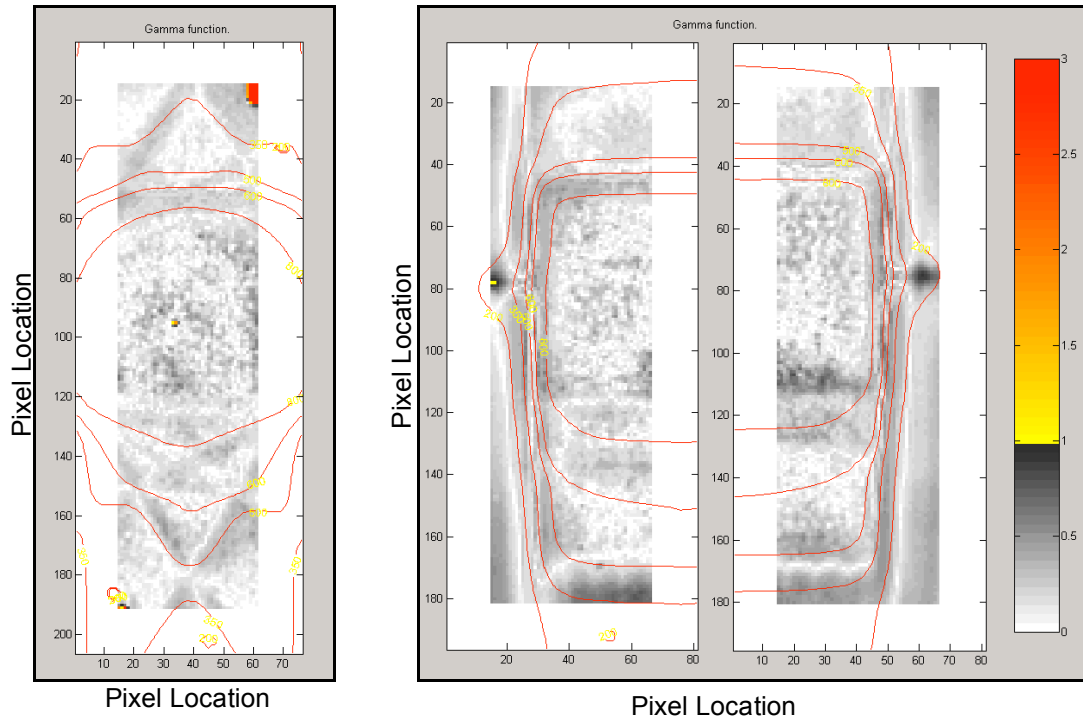


Figure 3.16: Gamma analysis maps of the axial and sagittal planes for the first trial of the conformal irradiation. The x and y axes are the pixel locations. The gamma value at each point is color coded according to the bar on the right of the figure. Due to small deviations in the image cropping and registration, the scale is not exactly the same for each portion of the figure.

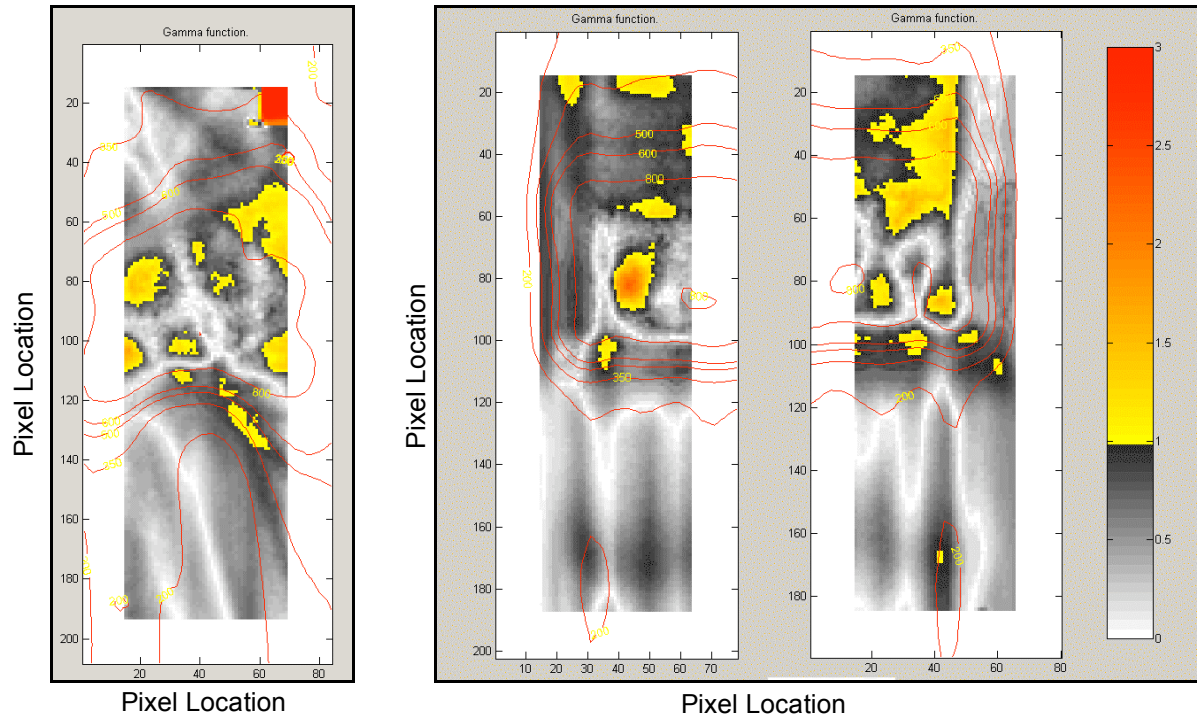


Figure 3.17: Gamma analysis maps of the axial and sagittal planes for the second trial of the IMRT #1 irradiation. The x and y axes are the pixel locations. The gamma value at each point is color coded according to the bar on the right of the figure. Due to small deviations in the image cropping and registration, the scale is not exactly the same for each portion of the figure.

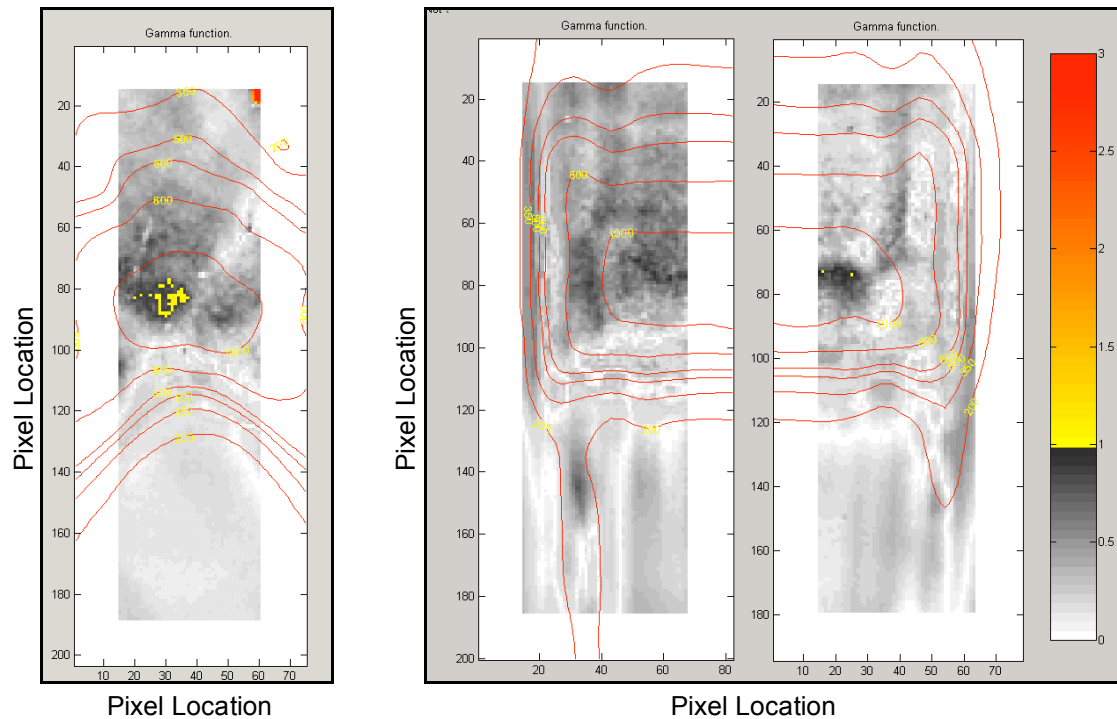


Figure 3.18: Gamma analysis maps of the axial and sagittal planes for the first trial of the IMRT #2 irradiation. The x and y axes are the pixel locations. The gamma value at each point is color coded according to the bar on the right of the figure. Due to small deviations in the image cropping and registration, the scale is not exactly the same for each portion of the figure.

Figures 3.15 – 3.18 are the gamma maps for single trials for the four-field box, conformal, IMRT #1, and IMRT #2 plans at the gamma criteria of 5% / 3 mm. The only failure patterns of note occurred on the IMRT plan #1 irradiation, when the irradiation was not well localized. On the IMRT plan #2 gamma maps, there were small regions of failure near the center of the high dose region on the axial plane; these regions were also apparent in the isodose distributions and axial dose profiles.

The following table shows the percentage of pixels, in each plane, that pass the criteria for each irradiation. Also included are the percentages of passing pixels at tighter gamma criteria. The tighter criteria are included because of the near perfect

agreement at the 5% / 3mm level for the four-field box, conformal, and IMRT plan #2 irradiations.

Mean Percentage of Passing Pixels

<i>Plan:</i>	<i>Plane:</i>	<i>5%/3mm</i>	<i>5%/2mm</i>	<i>3%/2mm</i>	<i>Sample Size</i>
<i>Box</i>	<i>Axial</i>	99.6	99.5	95.6	3
	<i>Sagittal</i>	99.3	99.3	95.4	3
<i>3-D Conformal</i>	<i>Axial</i>	99.4	99.3	97.9	3
	<i>Sagittal</i>	99.8	99.8	97.1	3
<i>IMRT #1</i>	<i>Axial</i>	93.3	80.2	63.3	2
	<i>Sagittal</i>	91.4	74.1	61.3	3
<i>IMRT #2</i>	<i>Axial</i>	99.6	98.7	94.4	3
	<i>Sagittal</i>	100	99.9	98.5	3

Table 3.5: The mean percentage of pixels passing the gamma criteria for each dose plane in each irradiation. Increasingly tighter criteria are shown in the table. Only 2 samples were available for the axial plane of the IMRT plan #1 due to an overexposure of one film to fluorescent light.

The threshold for good agreement across a dose plane is customarily that 95% of the pixels pass the selected criteria. The table indicates that for the three well localized plans (excluding IMRT plan #1, which was not well localized), there is nearly perfect agreement at the 5% / 3 mm level. The irradiation with a 2.5 mm shift, IMRT plan #1, shows slightly worse agreement, but is still above 90% agreement across the trials. When subjected to a distance criterion tighter than the positioning error (the positioning error was approximately 2.5 mm), the pixel passing percentage dropped precipitously, while the other trials maintained near perfect agreement. This finding suggests that the RPC may utilize a tighter distance to agreement criterion to better capture small positioning errors committed by institutions irradiating the spine phantom.

The results of the gamma analysis were consistent with a previous RPC study by Davidson et al., which found greater than 95% agreement across the gamma analysis

maps when using the Pinnacle dose engine to predict doses in a lung phantom (Davidson 2006).

Chapter 4 Conclusions and Future Work

4.1 Conclusions

The spine phantom is to be used to test institution's ability to scan, plan, and administer a stereotactic radiosurgical treatment. The dosimetric utility of the spine phantom was tested using a variety of irradiation plans, from unmodulated beams to clinically applicable IMRT plans. This project assessed the dosimetric agreement between the clinically utilized TPS at M.D. Anderson and the TLD/radiochromic film system implemented in the phantom.

The anatomy of the spine phantom was determined to closely emulate that of a patient with a similar chest breadth. The depth and size of the target volume and spinal canal were very similar to that of the sample patient, and the proximity of the spinal canal to the target volume did not exclude the spine phantom from RTOG 0631.

Using established 2-D dose plane comparison techniques, the planned and measured dose distributions showed excellent agreement in the four-field box, conformal, and IMRT plan #2 irradiations. The IMRT plan #1 irradiation did not pass the criteria set forth in this project, due to poor localization of the treatment isocenter during the treatment administration. This irradiation was included for illustrative purposes of the failure patterns for a poor localization.

The isodose distributions and axial dose profiles were first utilized to assess the agreement between the planned and administered dose across the axial and sagittal film

planes. For the four-field box, conformal, and IMRT plan #2 irradiations, the isodose distributions demonstrated agreement across the sagittal and axial film planes. For the IMRT #2 distributions, there was some disagreement at the high dose levels. This disagreement may warrant a revisiting of the film calibration at those higher dose levels, over 1000 cGy.

The results of the isodose distributions and dose profiles were consistent with studies conducted by the RPC for other anthropomorphic phantoms. Specifically, the collapsed-cone convolution dose calculation algorithm accurately calculated the measured dose across inhomogeneities. This project demonstrated that this assumption can be extended to the new spine phantom when irradiating with intensity modulated radiosurgical plans with small margins.

The gamma distributions for the four-field box, conformal, and IMRT plan #2 irradiations showed excellent agreement ($> 95\%$) in the gamma analyses at the 5% / 3 mm and 3% / 2 mm levels. The IMRT #1 irradiation showed lower levels of agreement at both criteria; this was expected, as the spine phantom was shifted 2.5 mm from the planned isocenter. The following chart summarizes the levels of agreement for the gamma maps for each irradiation:

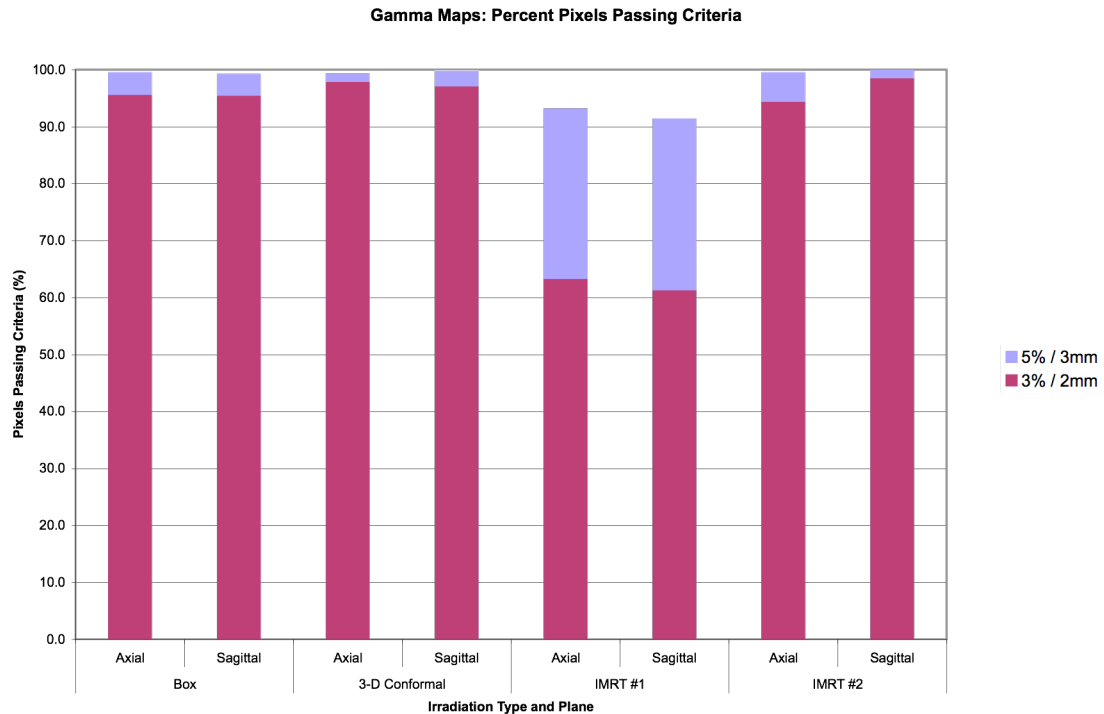


Figure 4.1: *The mean percentage of pixels passing the gamma criteria for each anatomic plane for each irradiation type.*

This figure demonstrates the greater than 95% agreement across each gamma map for the four field box, conformal and IMRT plan #2 irradiations at the 5% / 3 mm level. The tighter criteria also reflect excellent agreement for these irradiations. Visual inspection of the gamma maps and isodose distributions of the IMRT plan #1 irradiation reveal a clear shift; however, the number of pixels passing criteria is greater than 90% at the 5% / 3mm level. This reflects the relative laxity of that criterion; the 3% / 2mm criteria better capture the misadministration. Thus, when selecting criteria, it is important to consider the types and levels of errors tolerated, especially when considering the accuracy necessary for spinal radiosurgery. The limiting accuracy of the localization process used in this study should also be considered. The accuracy of the jaw positioning, per the

AAPM Task Group 142 report, is ± 1 mm for each jaw (Klein 2009). As both jaws are subject to this uncertainty, the localization uncertainty of the process used here is at least 1 mm.

This project demonstrated the dosimetric utility of the spine phantom for unmodulated and IMRT treatment plans for radiosurgical dose levels with proper localization. This project confirmed that the phantom is useful for assessing institutions participating in spinal radiosurgery protocols. The hypothesis, that the newly constructed spine phantom provided a useful model for planning intensity modulated radiosurgery for spinal tumors, and the collapsed-cone convolution dose algorithm accurately models the dose distributions measured via radiochromic film and TLD, was not rejected through testing in each specific aim of this research.

4.2 Future Work

This project applied to institutions that utilize conventional linear accelerators equipped with MLCs and planning systems that utilize a collapsed-cone convolution dose algorithm with heterogeneity correction, such as that implemented in the Pinnacle TPS. However, another technology used for external beam radiosurgery is the Cyberknife system, manufactured by Accuray (Sunnyvale, CA). Cyberknife utilizes a linear accelerator mounted on an articulating robotic arm with circular apertures. Cyberknife uses implanted gold fiducials and orthogonal kV imaging for localization. Accuray has recently upgraded its treatment planning software, MultiPlan®, from a pencil beam based calculation to a Monte Carlo dose algorithm (Mardirossian 2009). The RPC has already adapted a spine phantom for use with Cyberknife by placing gold fiducials into the spinal

insert. Future work may include generating plans in both versions of the Cyberknife treatment planning software, irradiating the spine phantom on a Cyberknife system, and using the criteria in this project to verify the dosimetric utility of the phantom for the Cyberknife system.

The RPC is also implementing optically stimulated luminescent (OSL) dosimeters in the place of TLD for remote dosimetry. The RPC's transition to OSL is ongoing, and the spinal insert could be adapted to Landauer's (Glenwood, IL) NanoDot® OSL cartridges.

Appendix

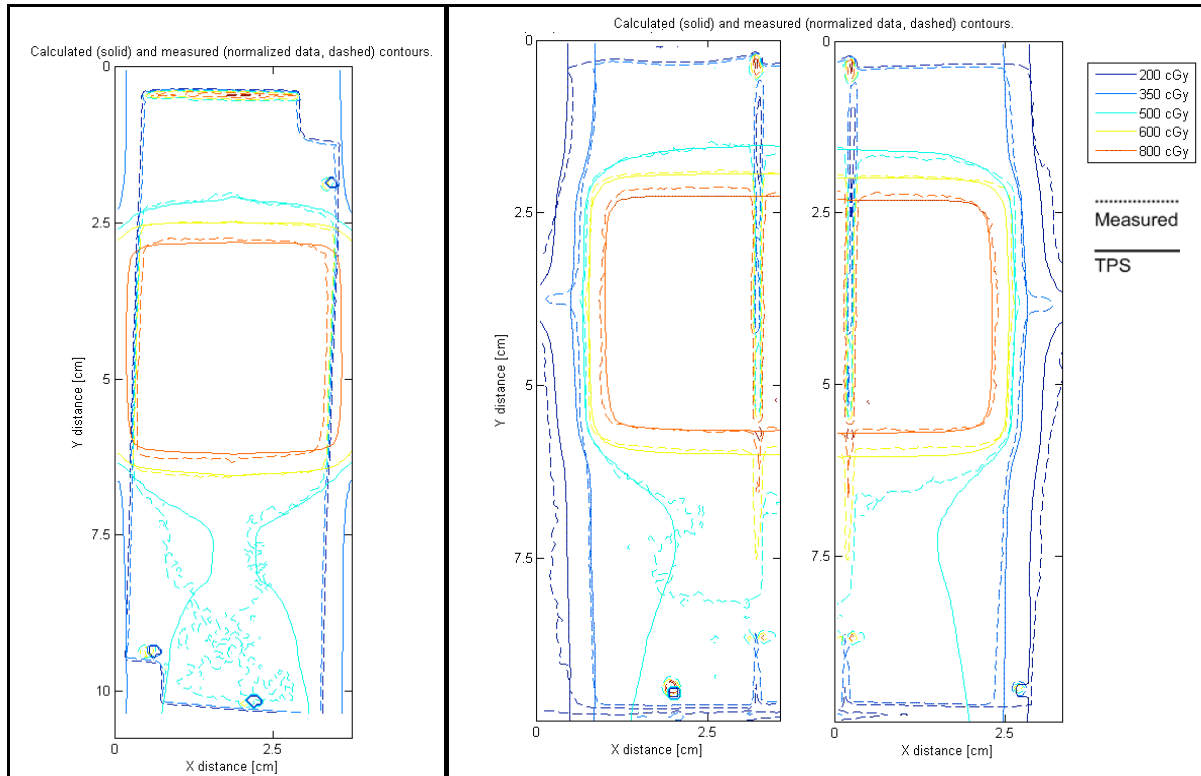


Figure 5.1: Isodose distributions for the axial and sagittal planes of the Four-Field Box irradiation, Trial 2. The figure shows, from left to right, the axial, inferior sagittal, and superior sagittal planes. Due to small deviations in the cropping and registration, the scale is not the same for each portion of the figure.

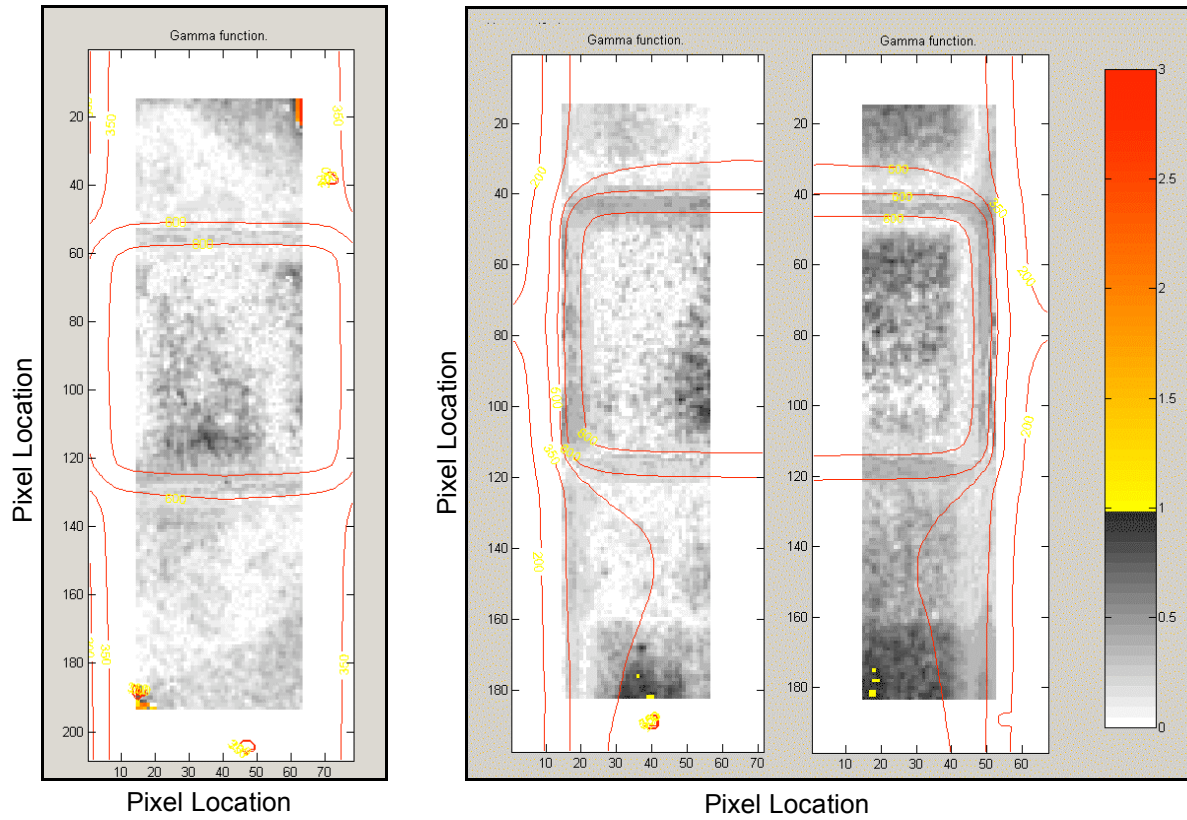


Figure 5.2: Gamma analysis maps of the axial and sagittal planes for the Four-Field Box irradiation, Trial 2. The x and y axes are the pixel locations. The gamma value at each point is color coded according to the bar on the right of the figure.

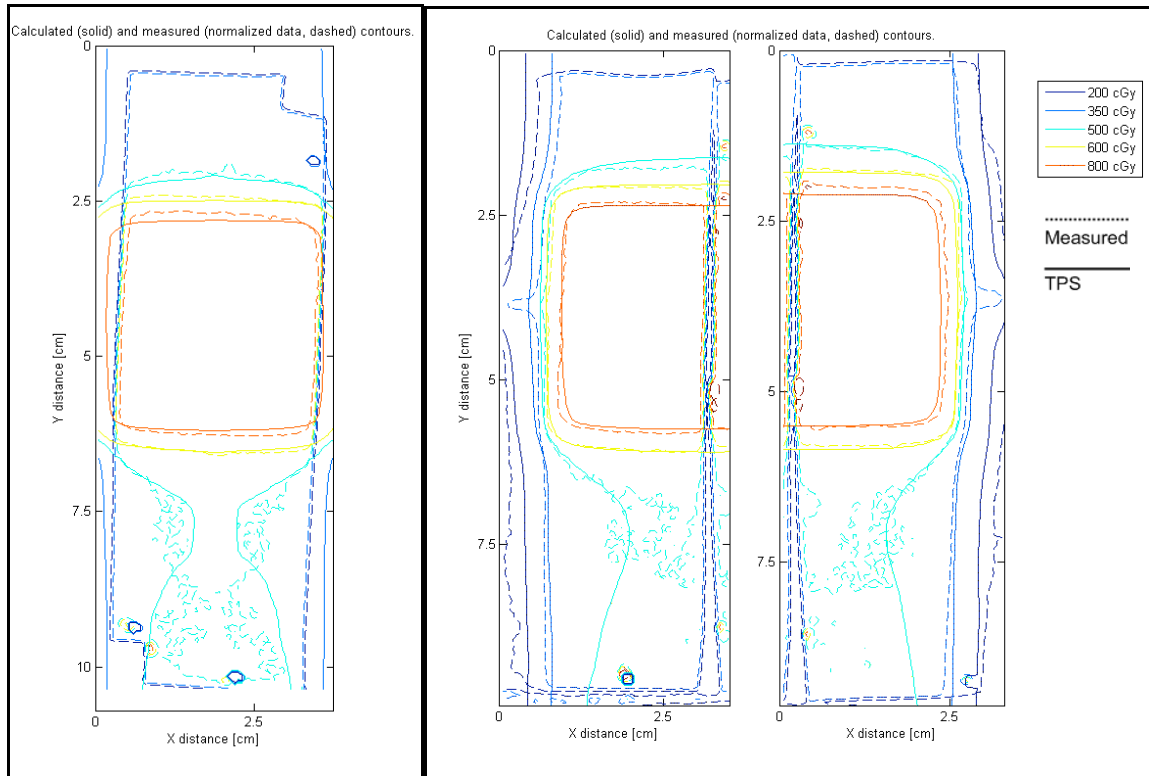


Figure 5.3: Isodose distributions for the axial and sagittal planes of the Four-Field Box irradiation, Trial 3. The figure shows, from left to right, the axial, inferior sagittal, and superior sagittal planes. Due to small deviations in the cropping and registration, the scale is not the same for each portion of the figure.

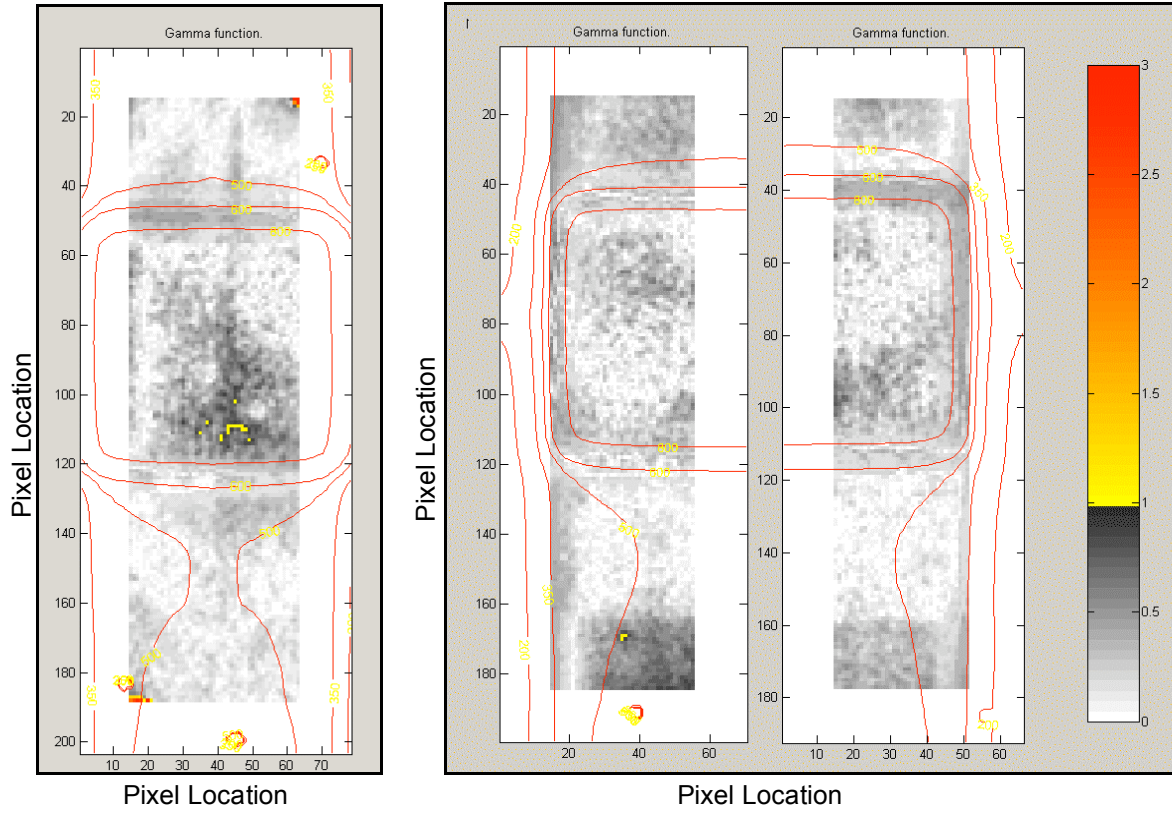


Figure 5.4: Gamma analysis maps of the axial and sagittal planes for the Four-Field Box irradiation, Trial 3. The x and y axes are the pixel locations. The gamma value at each point is color coded according to the bar on the right of the figure.

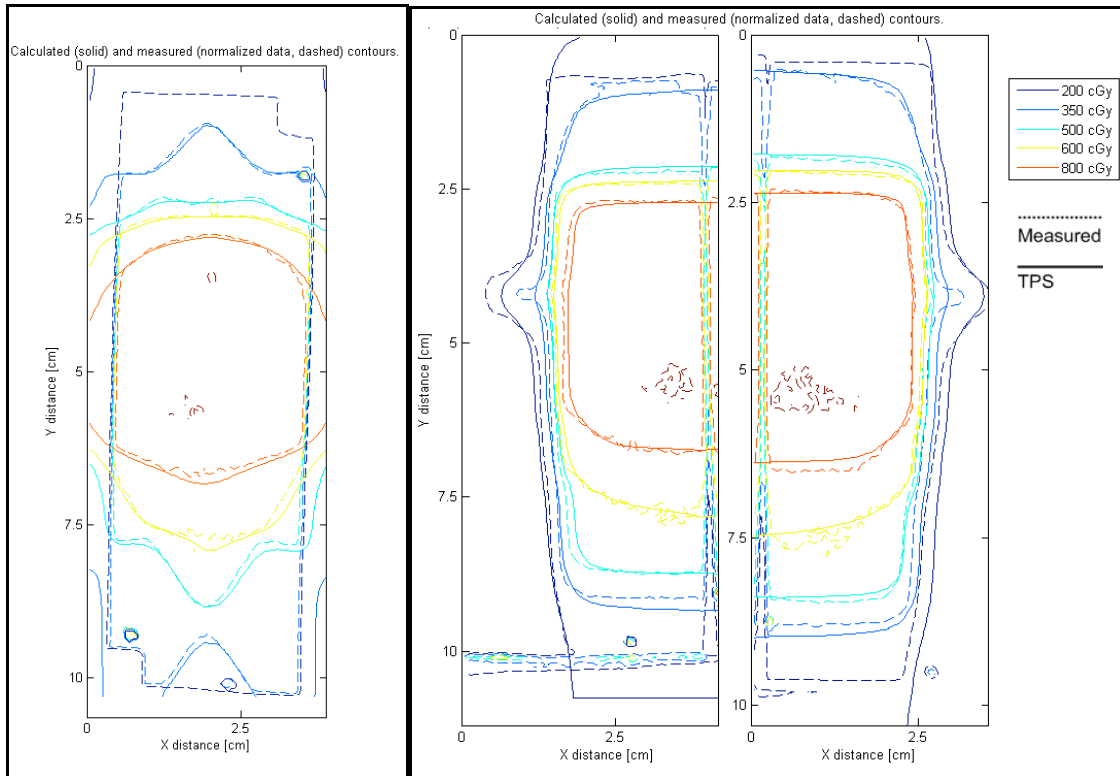


Figure 5.5: Isodose distributions for the axial and sagittal planes of the conformal irradiation, Trial 2. The figure shows, from left to right, the axial, inferior sagittal, and superior sagittal planes. Due to small deviations in the cropping and registration, the scale is not the same for each portion of the figure.

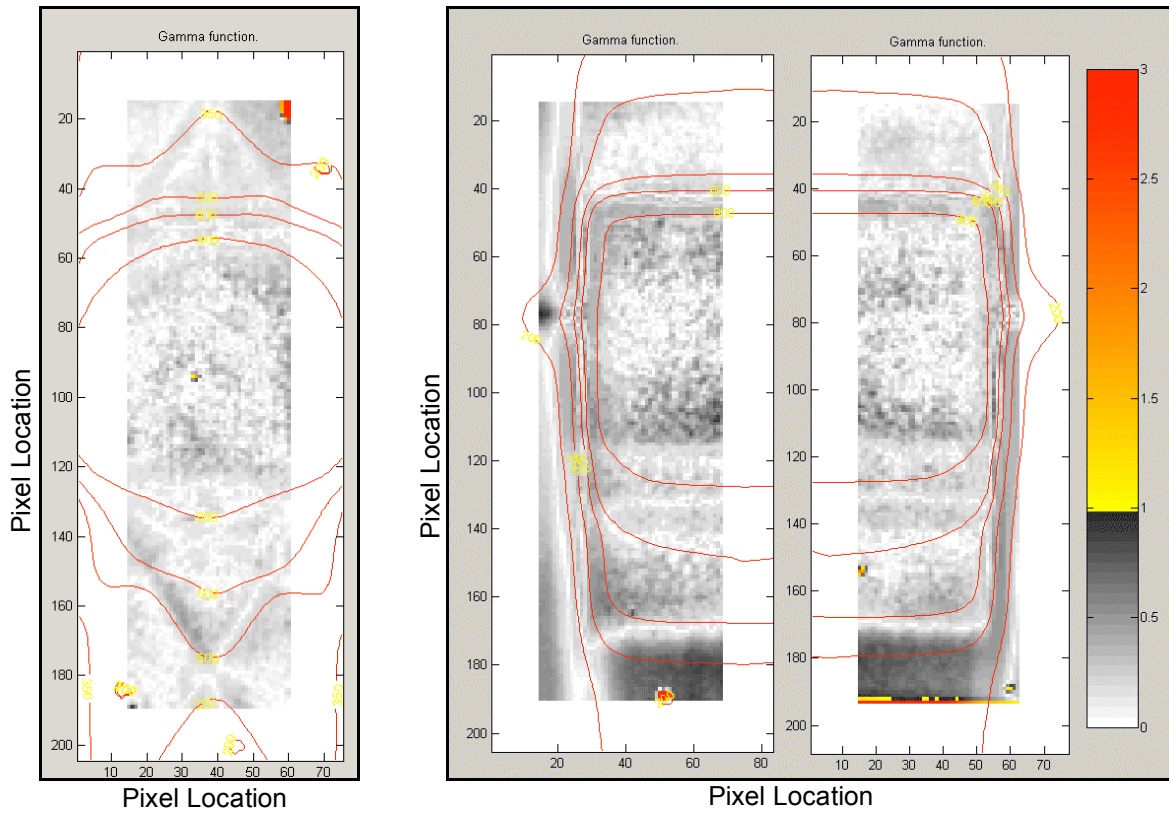


Figure 5.6: Gamma analysis maps of the axial and sagittal planes for the Conformal irradiation, Trial 2. The x and y axes are the pixel locations. The gamma value at each point is color coded according to the bar on the right of the figure.

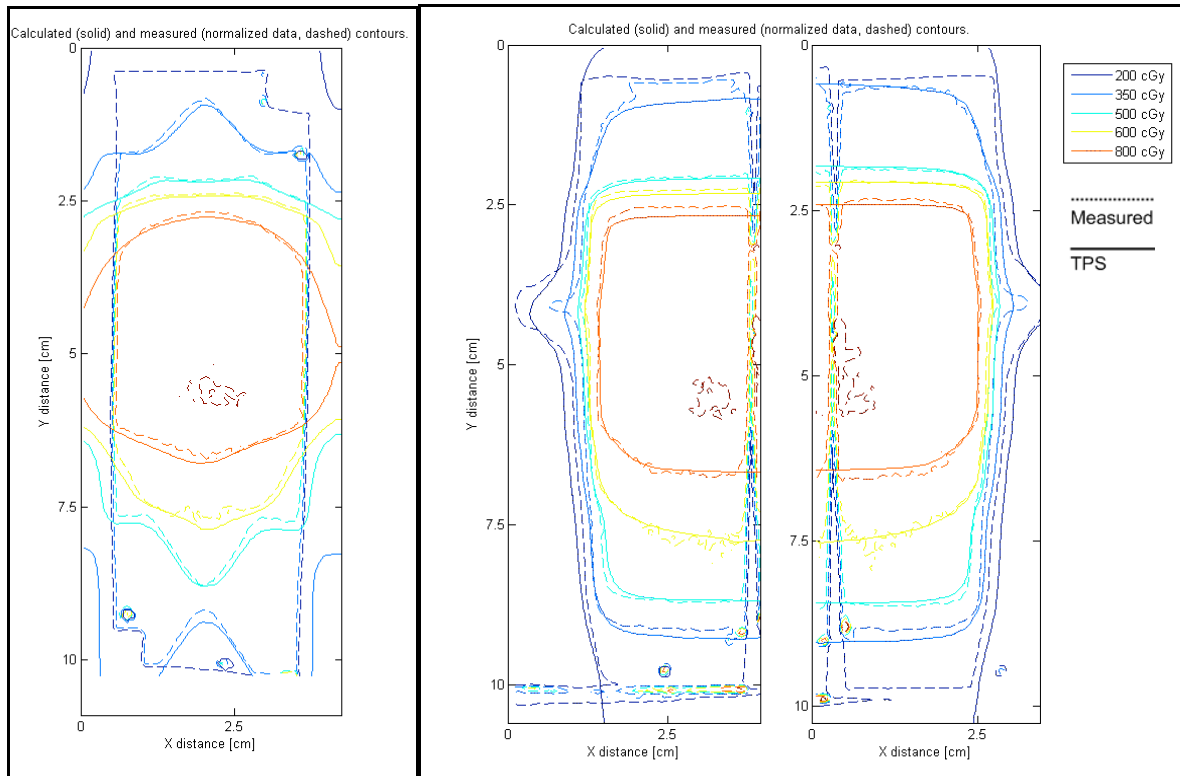


Figure 5.7: Isodose distributions for the axial and sagittal planes of the Conformal irradiation, Trial 3. The figure shows, from left to right, the axial, inferior sagittal, and superior sagittal planes. Due to small deviations in the cropping and registration, the scale is not the same for each portion of the figure.

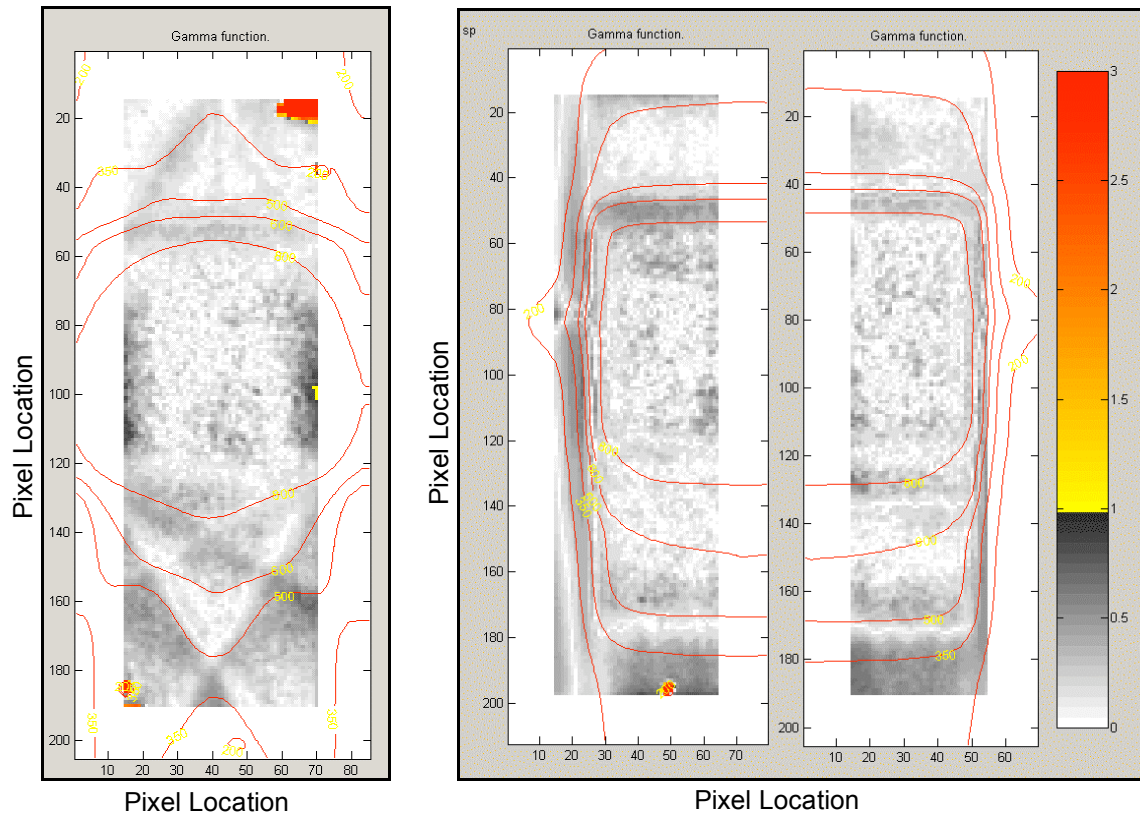


Figure 5.8: Gamma analysis maps of the axial and sagittal planes for the Conformal irradiation, Trial 3. The x and y axes are the pixel locations. The gamma value at each point is color coded according to the bar on the right of the figure.

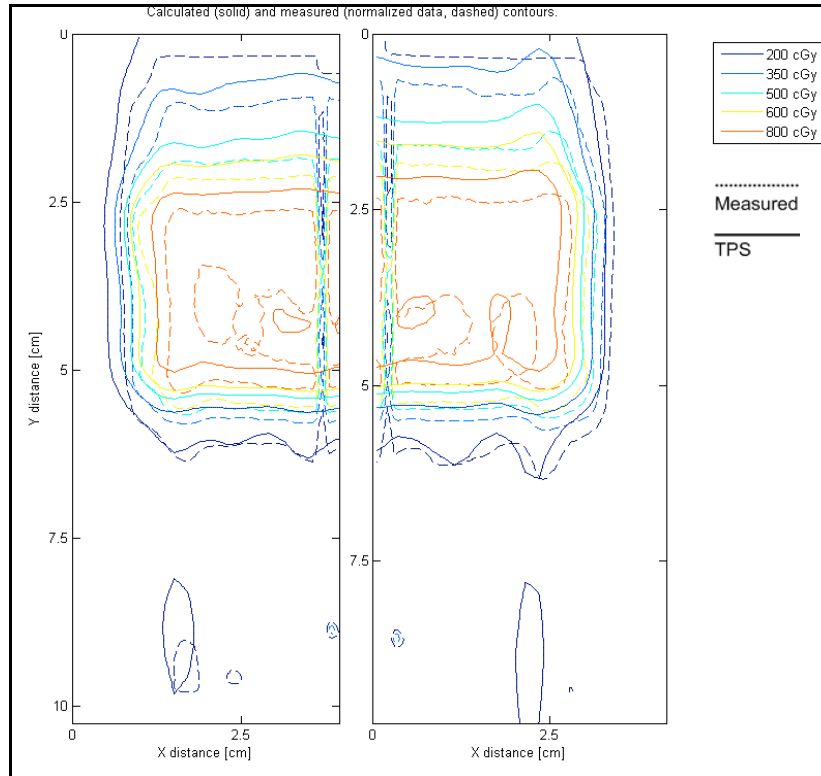


Figure 5.9: Isodose distribution of the sagittal plane of the IMRT #1 irradiation, Trial 1. The figure shows, from left to right, the inferior sagittal and superior sagittal planes. Due to small deviations in the cropping and registration, the scale is not the same for each portion of the figure.

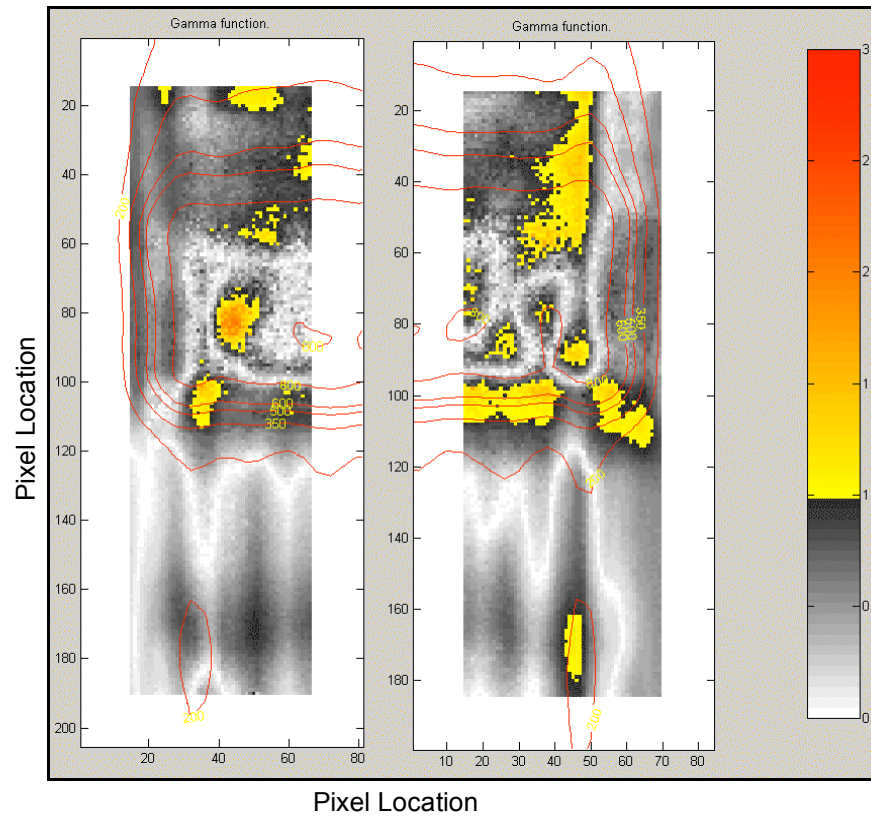


Figure 5.10: Gamma analysis map of the sagittal plane of the IMRT #1 irradiation, Trial 1. The x and y axes are the pixel locations. The gamma value at each point is color coded according to the bar on the right of the figure.

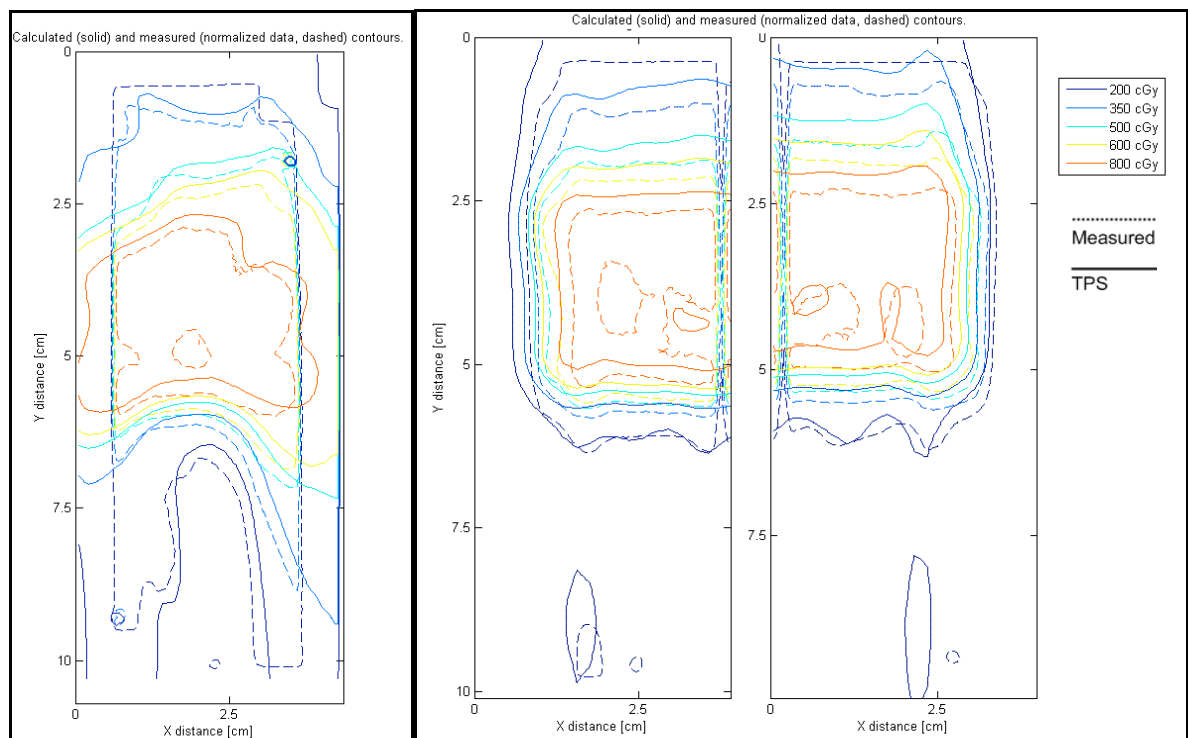


Figure 5.11: Isodose distributions for the axial and sagittal planes of the IMRT #1 irradiation, Trial 3. The figure shows, from left to right, the axial, inferior sagittal, and superior sagittal planes. Due to small deviations in the cropping and registration, the scale is not the same for each portion of the figure.

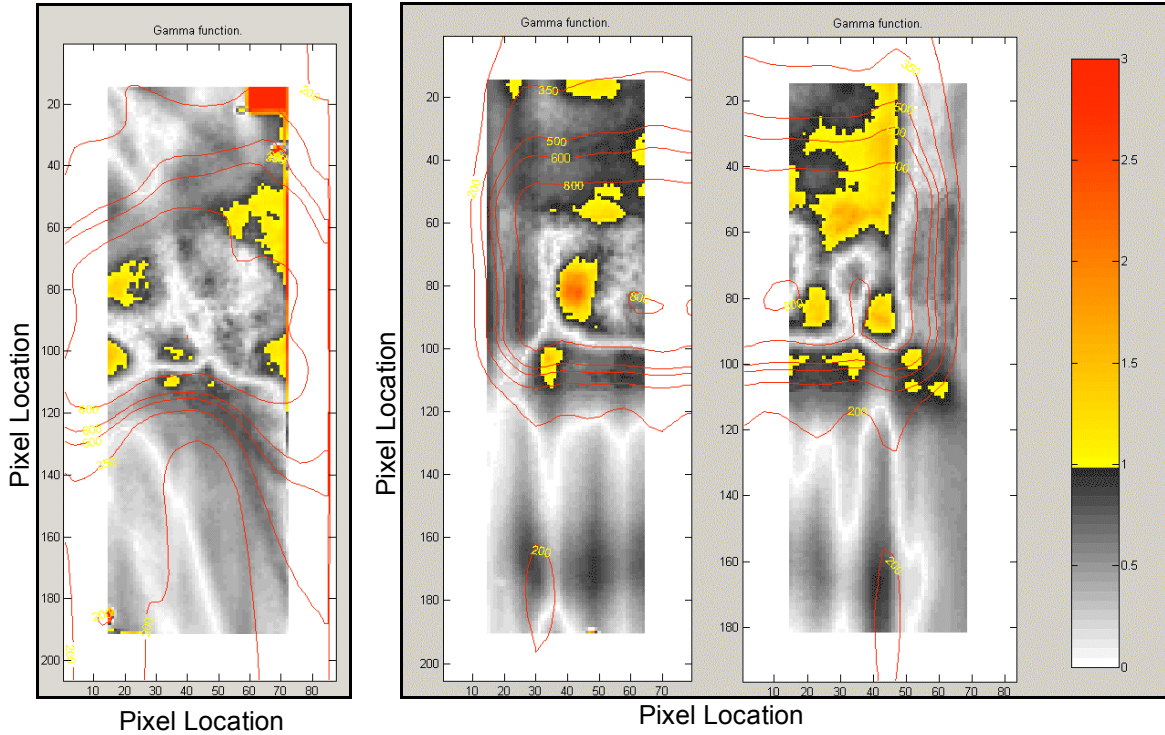


Figure 5.12: Gamma analysis maps of the axial and sagittal planes for the IMRT #1 irradiation, Trial 3. The x and y axes are the pixel locations. The gamma value at each point is color coded according to the bar on the right of the figure.

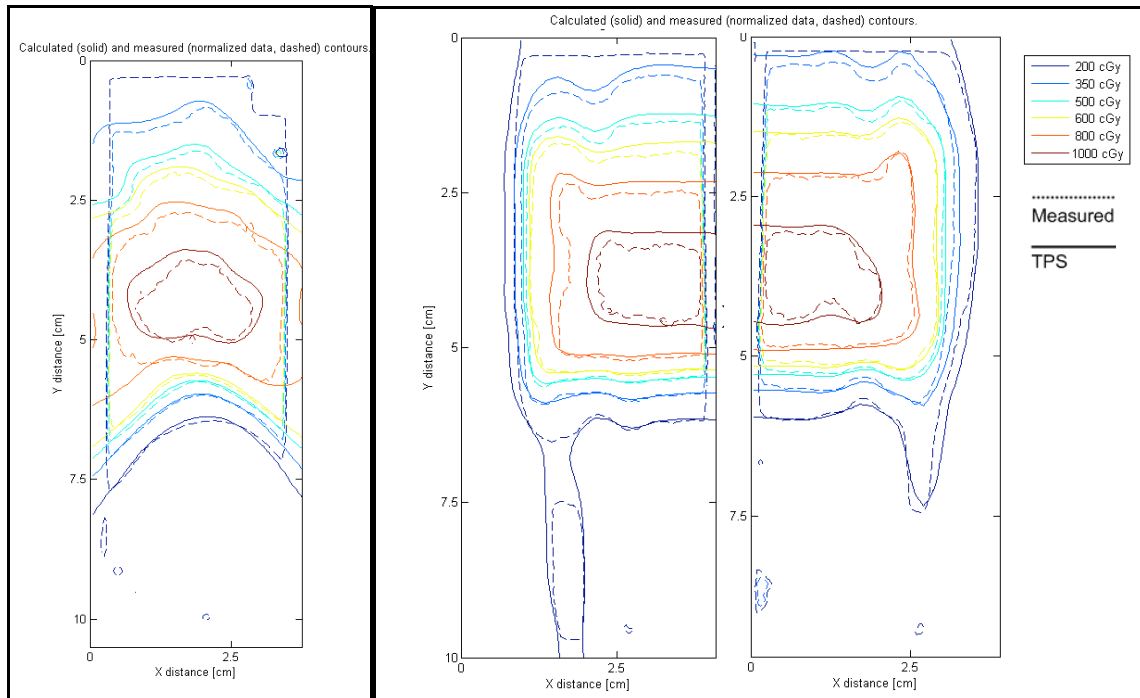


Figure 5.13: Isodose distributions for the axial and sagittal planes of the IMRT #2 irradiation, Trial 2. The figure shows, from left to right, the axial, inferior sagittal, and superior sagittal planes. Due to small deviations in the cropping and registration, the scale is not the same for each portion of the figure.

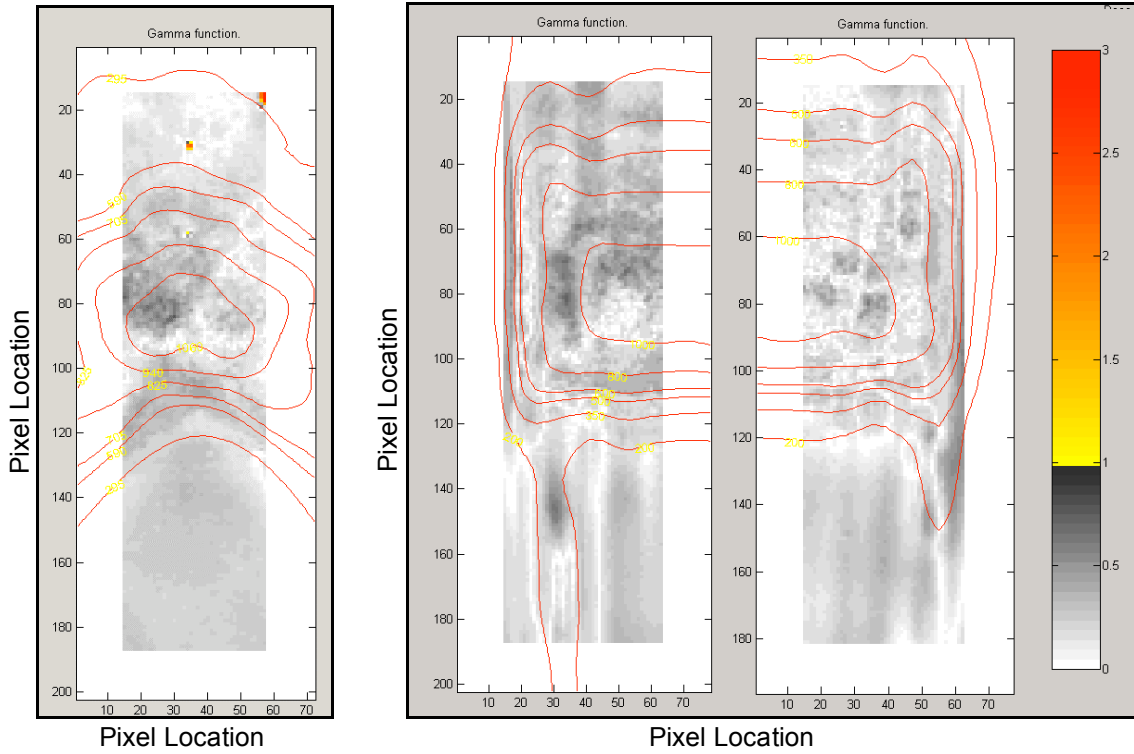


Figure 5.14: Gamma analysis maps of the axial and sagittal planes for the IMRT #2 irradiation, Trial 2. The x and y axes are the pixel locations. The gamma value at each point is color coded according to the bar on the right of the figure

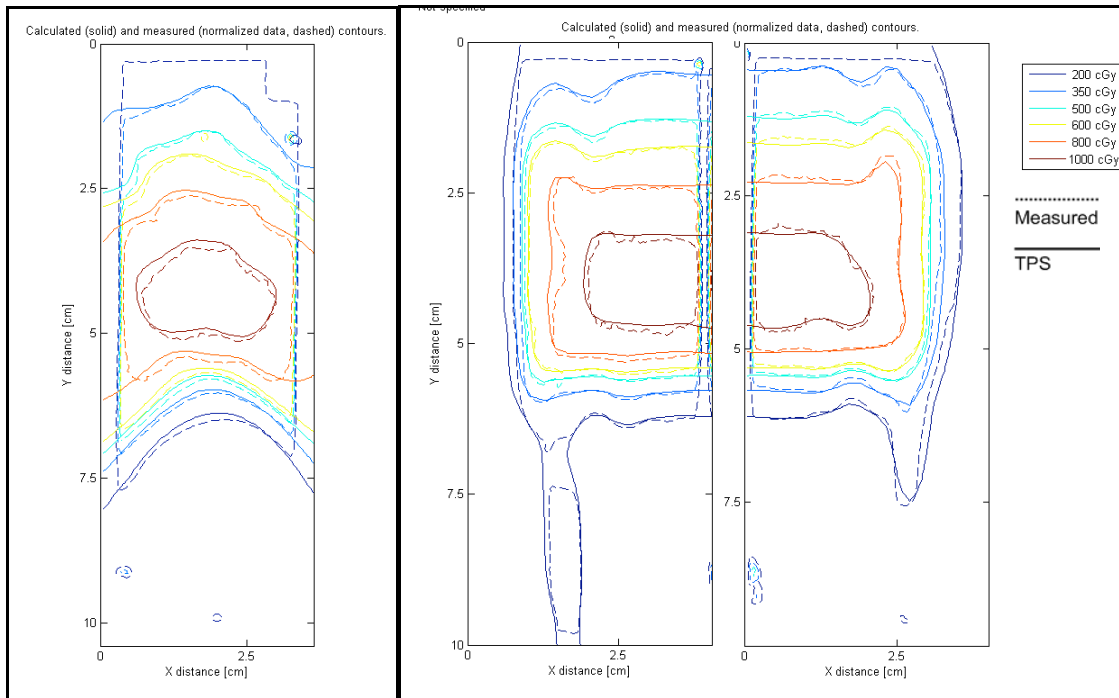


Figure 5.15: Isodose distributions for the axial and sagittal planes of the IMRT #2 irradiation, Trial 3.. The figure shows, from left to right, the axial, inferior sagittal, and superior sagittal planes. Due to small deviations in the cropping and registration, the scale is not the same for each portion of the figure.

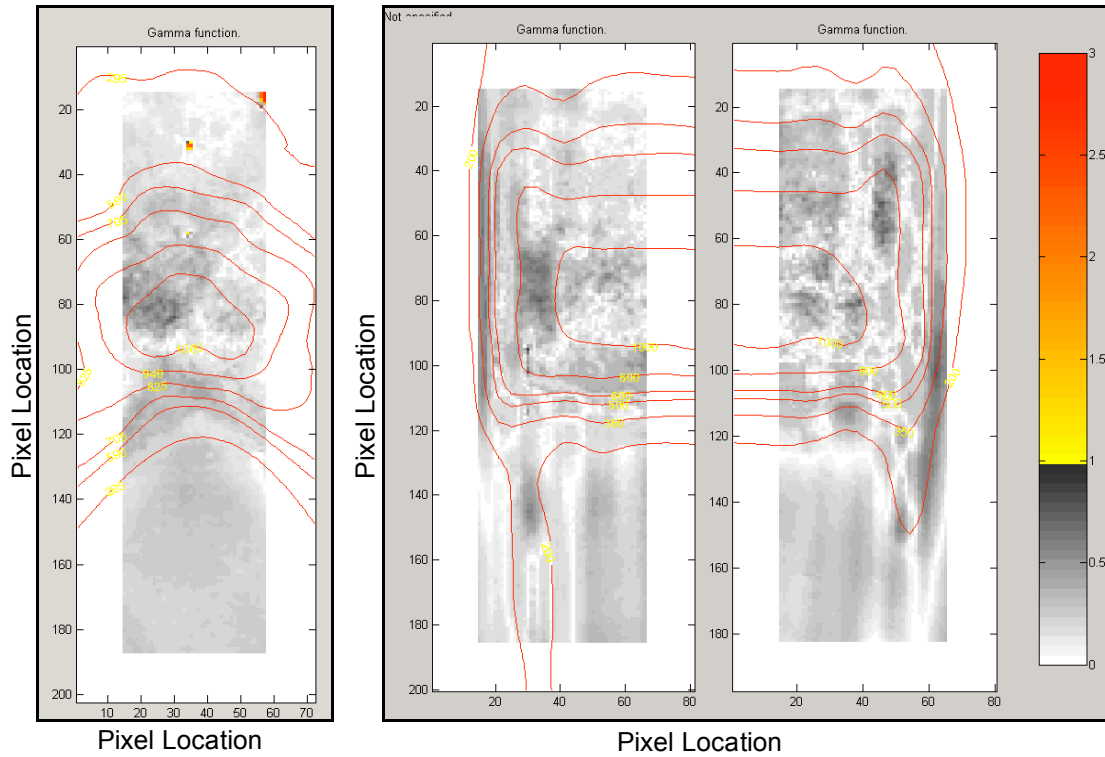


Figure 5.16: Gamma analysis maps of the axial and sagittal planes for the IMRT #2 irradiation, Trial 3. The x and y axes are the pixel locations. The gamma value at each point is color coded according to the bar on the right of the figure.

Bibliography:

- Chang, E. L., A. S. Shiu, E. Mendel, L. A. Mathews, A. Mahajan, P. K. Allen, J. S. Weinberg, B. W. Brown, X. S. Wang, S. Y. Woo, C. Cleeland, M. H. Maor and L. D. Rhines (2007). "Phase I/II study of stereotactic body radiotherapy for spinal metastasis and its pattern of failure." J Neurosurg Spine 7(2): 151-60.
- Childress, N. L., C. Bloch, R. A. White, M. Salehpour and Rosen, II (2005). "Detection of IMRT delivery errors using a quantitative 2D dosimetric verification system." Med Phys 32(1): 153-62.
- Davidson, S. E. (2006). Heterogeneity Dose Calculation Algorithm Accuracy in IMRT Using Anthropomorphic Thorax Phantom. Houston, The Graduate School of Biomedical Sciences.
- Dodd, R., I. C. Gibbs, J. R. Adler, Jr. and S. Chang (2008). Spinal Tumors. Principles and Practice of Stereotactic Radiosurgery. L. Chin and W. Regine. New York, Springer: 431-433.
- Gerszten, P. C., S. A. Burton, C. Ozhasoglu and W. C. Welch (2007). "Radiosurgery for spinal metastases: clinical experience in 500 cases from a single institution." Spine (Phila Pa 1976) 32(2): 193-9.
- Holder, A. and B. C. Salter (2004). A tutorial on radiation oncology and optimization. Emerging Methodologies and Applications in Operations Research. H. Greenberg. Boston, Kluwer Academic Press.
- Kirby, T. H., W. F. Hanson and D. A. Johnston (1992). "Uncertainty analysis of absorbed dose calculations from thermoluminescence dosimeters." Med Phys 19(6): 1427-33.

- Klein, E. E., J. Hanley, J. Bayouth, F. F. Yin, W. Simon, S. Dresser, C. Serago, F. Aguirre, L. Ma, B. Arjomandy, C. Liu, C. Sandin and T. Holmes (2009). "Task Group 142 report: quality assurance of medical accelerators." Med Phys **36**(9): 4197-212.
- Klimo, P., Jr. and M. H. Schmidt (2004). "Surgical management of spinal metastases." Oncologist **9**(2): 188-96.
- Low, D. A., W. B. Harms, S. Mutic and J. A. Purdy (1998). "A technique for the quantitative evaluation of dose distributions." Med Phys **25**(5): 656-61.
- Mardirossian, G., C. Lee, M. Muniruzaman and H. Jin (2009). Validation of Accuray MultiPlan Monte Carlo Treatment Plans. 2009 CyberKnife Users' Meeting, Hollywood, FL.
- Medin, P. and D. verellen (2006). Novalis. Extracranial Stereotactic Radiotherapy and Radiosurgery. B. Slotman, T. Solberg and D. Verellen. New York, Taylor & Francis Group: 54-55.
- Molineu, A., D. S. Followill, P. A. Balter, W. F. Hanson, M. T. Gillin, M. S. Huq, A. Eisbruch and G. S. Ibbott (2005). "Design and implementation of an anthropomorphic quality assurance phantom for intensity-modulated radiation therapy for the Radiation Therapy Oncology Group." Int J Radiat Oncol Biol Phys **63**(2): 577-83.
- RTOG (2009). RTOG 0631 Phase II/III Study of Image-Guided Radiosurgery/SBRT for Localized Spine Metastasis.
<http://www.rtog.org/members/protocols/0631/0631.pdf>.

- Ryu, S. and P. C. Gerszten (2009). Target Delineation and Dose Prescription. Spinal Radiosurgery. S. Ryu and P. C. Gerszten. New York, Thieme: 73-75.
- Ryu, S., R. Jin, J. Y. Jin, Q. Chen, J. Rock, J. Anderson and B. Movsas (2008). "Pain control by image-guided radiosurgery for solitary spinal metastasis." J Pain Symptom Manage **35**(3): 292-8.
- Schell, M., F. Bova, D. Larson, D. Keavett, W. Lutz, E. Podgorsak and A. Wu (1995). Stereotactic Radiosurgery. AAPM Task Group 42 Report. Boston, American Association of Medical Physicists. **54**.
- Yin, F. F., S. Ryu, M. Ajlouni, J. Zhu, H. Yan, H. Guan, K. Faber, J. Rock, M. Abdalhak, L. Rogers, M. Rosenblum and J. H. Kim (2002). "A technique of intensity-modulated radiosurgery (IMRS) for spinal tumors." Med Phys **29**(12): 2815-22.

Vita

Douglas Caruthers was born in Los Angeles, California on April 15th 1983 to Rex and Anna Caruthers. He has three brothers, Kent, Tyrone, and William. He graduated from Washington University in St. Louis in 2005 with a B.S. in Biomedical Engineering. He worked for BrainLAB Inc. as a Field Service Engineer before entering the University of Texas Health Science Center at Houston Graduate School of Biomedical Sciences. He enjoys reading, frisbee, and cooking.

Permanent address:

227 Straightoak Ct.

Ballwin, MO 63021